TABLE 4. Agreement between Heidelberg Retina Tomograph II-Moorfield's Regression Analysis and Clinical Diagnosis

	Sensitivity (95% Confidence Interval)	Specificity (95% Confidence Interval)	Positive Predictive Value (95% Confidence Interval)	Negative Predictive Value (95% Confidence Interval)
Person-level analysis (n=977)				
MRA 1	43/47(91.5%, 84.6-88.8)	781/930(84.0%, 77.2-82.2)	43/192(22.4%, 19.8-25.0)	781/785(99.5%, 99.1-99.9)
MRA 2	34/47(72.3%, 63.8-69.6)	866/930(93.1%, 88.1-91.9)	134/98(34.7%, 31.7-37.7)	866/879(98.5%, 97.8-99.2)
Eye-level analysis (Right eye & Left eye, n=2053)				
MRA 1	53/73(72.6%, 70.7-74.5)	1777/1980(89.7%, 88.4-91.0)	53/256(20.7%,18.9-22.5)	1777/1980(98.9%, 98.4-99.4)
MRA 2	44/73(60.3%, 58.2-62.4)	1896/1980(95.6%, 94.7-96.5)	44/128(34.4%, 32.3-36.5)	1896/1980(98.5%, 98.0-99.0)
Right eye (n=1029)				
MRA 1	25/36(69.4%, 66.6-72.2)	900/993(90.6%, 88.4-92.4)	25/118(21.2%, 18.7-23.7)	900/911(98.8%, 98.1-99.5)
MRA 2	20/36(55.6%, 52.6-58.6)	955/993(96.2%, 95.0-97.4)	20/58(34.5%, 31.6-37.4)	955/971(98.4%, 97.6-99.2)
Left eye (n=1024)				
MRA 1	28/37(75.7%, 73.1-78.3)	877/987(88.9%, 88.4-91.0)	28/138(20.3%, 17.7-22.9)	877/886(99.0%, 98.4-99.6)
MRA 2	24/37(64.9%, 62.0-67.8)	941/987(95.3%, 94.7-96.5)	24/70(34.3%, 31.4-37.2)	941/954(98.6%, 97.9-99.3)

MRA: Moorfield's Regression Analysis

MRA 1: "Borderline" outcomes were treated as test positive, MRA 2: "Borderline" outcomes were treated as test negative

In Vivo Imaging and Quantitative Evaluation of the Rat Retinal Nerve Fiber Layer Using Scanning Laser Ophthalmoscopy

Ichiro Kawaguchi, Tomomi Higashide, Shinji Ohkubo, Hisashi Takeda, and Kazuhisa Sugiyama

Purpose. To determine whether scanning laser ophthalmoscopy (SLO) is useful for in vivo imaging and quantitative evaluation of rat retinal nerve fiber layer (RNFL) using an optic nerve crush model.

Methods. The optic nerve of the right eye was crushed intraorbitally with a clip. The left eye served as the untreated control. Fundus images of both eyes were recorded by SLO using an argon blue laser before and 1, 2, and 4 weeks after optic nerve crush. The focused plane was sequentially moved by changing the refractive values in the SLO setting. The range of refractive values (ΔF) in which the RNFL reflex was clearly observed was determined. The RNFL thickness in retinal sections was measured and compared to the ΔF value from SLO images taken before histologic preparation.

Results. Striations of RNFL radiating from the optic disc were clearly visible by SLO. No obvious changes in the RNFL reflex were observed 1 week after optic nerve crush. However, striations of RNFL became uniformly darker and thinner 2 weeks after the crush and were barely visible 4 weeks after the crush. The ΔF value was unchanged 1 week after the crush, but then decreased significantly and progressively after the second week. ΔF was unchanged in the control eyes during the experimental period. The ΔF value correlated significantly with the histologically determined RNFL thickness.

Conclusions. SLO is a useful and valuable tool for in vivo imaging and quantitative evaluation of rat RNFL. (*Invest Ophthalmol Vis Sci.* 2006;47:2911-2916) DOI:10.1167/iovs.05-1169

Retinal nerve fiber layer (RNFL) defects are one of the most critical factors to assess in the evaluation of the degree and distribution of retinal ganglion cell loss in patients with glaucoma. In routine fundus examinations, red-free or green light rather than white light is suitable for visualization of RNFL, because of the optical properties of RNFL.[1] A scanning laser ophthalmoscope (SLO; Rodenstock Instruments, Munich, Germany) provides argon blue laser illumination and confocal apertures which are ideal for RNFL observation as the wavelength of the laser is optimal for RNFL visualization, and a small confocal aperture allows high-contrast imaging by reducing the scattered light arising from defocused tissues.[2] Accordingly, highly reproducible RNFL evaluation can be performed by SLO.[2] However, there are no detailed reports on RNFL in rat eyes visualized with an SLO, although in one study an SLO was used for imaging the rat fundus and assessing retinal circulation.[3]

Ocular hypertension, ischemia-reperfusion, and optic nerve crush rodent models have been used to elucidate the pathophysiology of glaucoma and other optic neuropathies.[4] In these models, loss of retinal ganglion cells has usually been evaluated histologically by counting the number of cell bodies in the retina or their axons in the optic nerve.[5-8] For intraretinal axons of retinal ganglion cells, qualitative assessment of the effect of axotomy has been performed by staining the axons in the flatmount retina.[6,9] However, there have been no reports of in vivo evaluation of RNFL changes in rodent models of optic nerve injury.

In this study, we determined whether the SLO is useful for in vivo imaging and quantitative evaluation of the rat RNFL using the optic nerve crush model.

Methods

Animals

Male Brown Norway rats, 12 weeks of age and weighing 200 to 250 g, were used in this study. The rats had free access to food and water and were maintained in cages in an environmentally controlled room with a 12-hour light-dark cycle. All experiments were conducted on rats anesthetized by an intraperitoneal injection (65 mg/kg) of sodium pentobarbital (Somnopentil; Schering-Plough Animal Health, Omaha, NE). All animals were treated in accordance with the ARVO statement for the Use of Animal in Ophthalmic and Vision Research.

Optic Nerve Crush Model

The conjunctiva of the right eye was incised in the supratemporal quadrant to expose the optic nerve by careful blunt dissection under an operating microscope. The optic nerve was crushed 2 mm behind the globe for 30 seconds with a 60-g vascular clip (Micro Vascular Clip; Roboz Surgical Instrument Co., Gaithersburg, MD). Special care was taken not to damage the blood supply to the eye traveling along the inferior side of the optic nerve.[10] Immediate recovery of retinal blood supply after removal of the clip was observed by indirect ophthalmoscopy in each eye. The left eye served as the untreated control.

In Vivo Imaging of RNFL over Time Using SLO

Before and 1, 2, and 4 weeks after optic nerve crush, the retinal images of both eyes were recorded by SLO (SLO 101; Rodenstock Instruments) with argon blue laser illumination (wavelength: 488 nm, output: 190-210 μW) in 21 rats. The eyes were dilated with 0.5% tropicamide and 0.5% phenylephrine hydrochloride eye drops (Santen Pharmaceuticals, Osaka, Japan). To preserve corneal clarity throughout the experiment, a custom-made contact lens with a radius of curvature

From the Department of Ophthalmology, Kanazawa University Graduate School of Medical Science, Kanazawa, Japan.

Supported by a Grant-in-Aid for Scientific Research from the Ministry of Education, Science, and Culture, Japan.

Submitted for publication September 1, 2005; revised February 3 and March 5, 2006; accepted May 1, 2006.

Disclosure: **I. Kawaguchi**, None; **T. Higashide**, None; **S. Ohkubo**, None; **H. Takeda**, None; **K. Sugiyama**, None

The publication costs of this article were defrayed in part by page charge payment. This article must therefore be marked "*advertisement*" in accordance with 18 U.S.C. §1734 solely to indicate this fact.

Corresponding author: Ichiro Kawaguchi, Department of Ophthalmology, Kanazawa University Graduate School of Medical Science, 13-1 Takara-machi, Kanazawa, Ishikawa 9208641 Japan; ichiro-k@mub.biglobe.ne.jp.

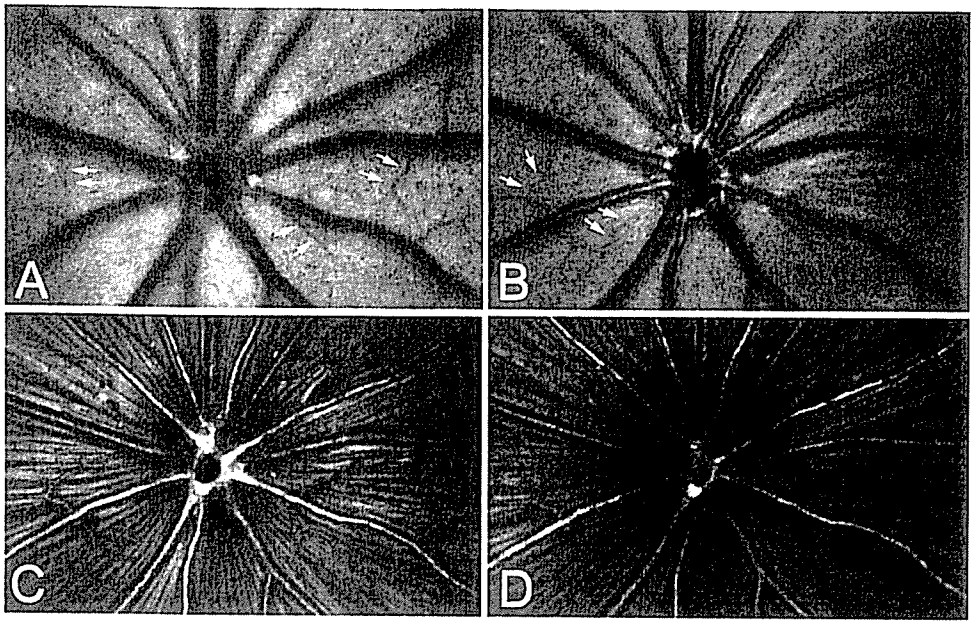

FIGURE 1. SLO images of normal rat fundus recorded under argon blue laser illumination through the narrowest confocal aperture. The focused plane was sequentially moved from sclerad (**A**) to vitread (**D**) by changing the refractive values (ΔF) in the SLO setting. (**A**) Refractive value, −8 D. White mottled reflex from the retinal pigment epithelium was prominent. Striations of RNFL are not visible. (**B**) Refractive value, −4 D. Radial striations of RNFL became visible. (**C**) Refractive value, +3 D. The striations of RNFL reflex were prominent. The dark area around the optic disc increased in size with larger refractive values than with this one. (**D**) Refractive value, +5 D. The large dark area around the optic disc indicates that the focused plane was in front of the retinal surface. In this case, the range of refractive values in which radial striations of RNFL are clearly observed near the optic disc is from −4 D to +3 D, and thus ΔF is 7 D. The pattern of retinal vessels in the SLO images (**A** vs. **B**, *arrows*) of the same retinal area are different at different focal planes, a finding that confirms the ability of the SLO for optical sectioning of rat retina using a 488-nm laser.

of 2.75 mm and a diameter of 5.0 mm (Kyoto Contact Lens, Kyoto, Japan) was placed on the cornea after topical anesthesia with 0.4% oxybuprocaine hydrochloride eye drops (Santen Pharmaceuticals). A rat was placed on a heating pad (Deltaphase Isothermal Pad; Braintree Scientific, Inc., Braintree, MA) and its head was gently held manually to keep the eye in position for illuminating the fundus evenly with the argon blue laser.

Fundus images with a field angle of 40° were recorded by digital video (GV-D1000; Sony Co., Tokyo, Japan). First, the widest confocal aperture (C3) was used for qualitative observation of RNFL. Then, for the quantitative evaluation of RNFL thickness, the narrowest confocal aperture (C1) was used to maximize the image contrast of the focused plane and the axial resolution. The focused plane was sequentially moved through the retina, sclerad to vitread, by changing the refractive values (maximum range, −20 D to +20 D) in the SLO setting (i.e., altering the setting of the ametropic corrector). The fundus images were recorded with a nominal 1-D step and the range of refractive values (ΔF) for RNFL thickness was determined by a masked observer.

As the focus measurements in this study were subjective, representative SLO images of RNFL with different focused planes, as shown in Figure 1, were used as the reference images for determining ΔF. For all 1-D steps of SLO images of each rat fundus, we looked carefully at the retinal location, approximately 1 disc diameter apart from the edges of the optic disc and determined the most sclerad focal plane where the radial striations of RNFL become just visible. We also determined the most vitread focal plane with the striations of RNFL reflex just before being covered by the dark area around the optic disc which enlarges with larger refractive values. For evaluation of the reproducibility and reliability of these subjective focus measurements, we calculated intra- and interobserver agreement in the measurements using the SLO image series of 24 rat fundi (six image series each at baseline and 1, 2, and 4 weeks after the optic nerve crush). Two observers independently determined ΔF for each rat fundus. The image series were presented in a random sequence on two separate occasions. The κ statistic was 0.92 and 0.83 for intra- and interobserver agreement respectively, indicating that reproducibility of the focus measurements was relatively good.

For each rat, we examined the fundus by indirect ophthalmoscopy after SLO imaging to ensure that visibility of the fundus was not compromised by the optic nerve crush surgery or other problems that may cause corneal opacity or cataract.

Correlation of ΔF and Histologically Determined RNFL Thickness

Sixteen rats were divided into four groups (four rats in each group). An optic nerve crush was performed in the right eye in three groups. Retinal sections of the right eye were prepared for RNFL thickness measurement at 1, 2, and 4 weeks after optic nerve crush. One group of rats was used for each time point. For baseline data, the optic nerve was not crushed in the remaining group of rats, and the right eye was processed similarly. Immediately after the recording of the fundus by SLO, the eyes were enucleated after administration of an anesthetic overdose of intraperitoneal pentobarbital sodium. The anterior segment was removed and a small marking cut was placed on the edge of the posterior eye cup to identify the superior retinal portion. The eye cup was fixed in 4% paraformaldehyde-0.5% glutaraldehyde and 0.1 M phosphate-buffered saline for 2 hours at room temperature, and was embedded in mounting compound (Tissue-TeK OCT; Sakura Finetechnical, Tokyo, Japan) followed by freezing with dry ice. Serial frozen sections (16 μm thick) were collected along the vertical meridian of the globe. After they were stained with hematoxylin-eosin, the retinal sections were observed under an optical microscope (Eclipse TE300; Nikon Corp., Kanagawa, Japan) and were recorded as JPEG files with a digital cooled CCD camera (DS-5Mc-L1; Nikon) and a personal computer (Dimension 8300; Dell Inc., Round Rock, TX). For each eye, RNFL thickness of three consecutive sections derived from a location approximately 500 μm temporal from the center of the optic disc (~1 disc diameter from the edge of the optic disc) was measured using image-analysis software (Image-Pro Express 4.0; MediaCybernetics, Inc., Silver Spring, MD) and averaged. The RNFL thickness in the retinal sections was compared by the ΔF determined from SLO images.

We also counted the number of cells in the ganglion cell layer in the retinal sections used for RNFL thickness measurements and calculated the mean number of cells in each eye.

Statistical Analysis

The difference in ΔF was analyzed by the Wilcoxon signed-rank test for comparison between control and crushed eyes and by the Friedman test and post hoc tests for comparison of ΔF measured at different time points. The differences in RNFL thickness and the number of cells in the ganglion cell layer in retinal sections at different time points were

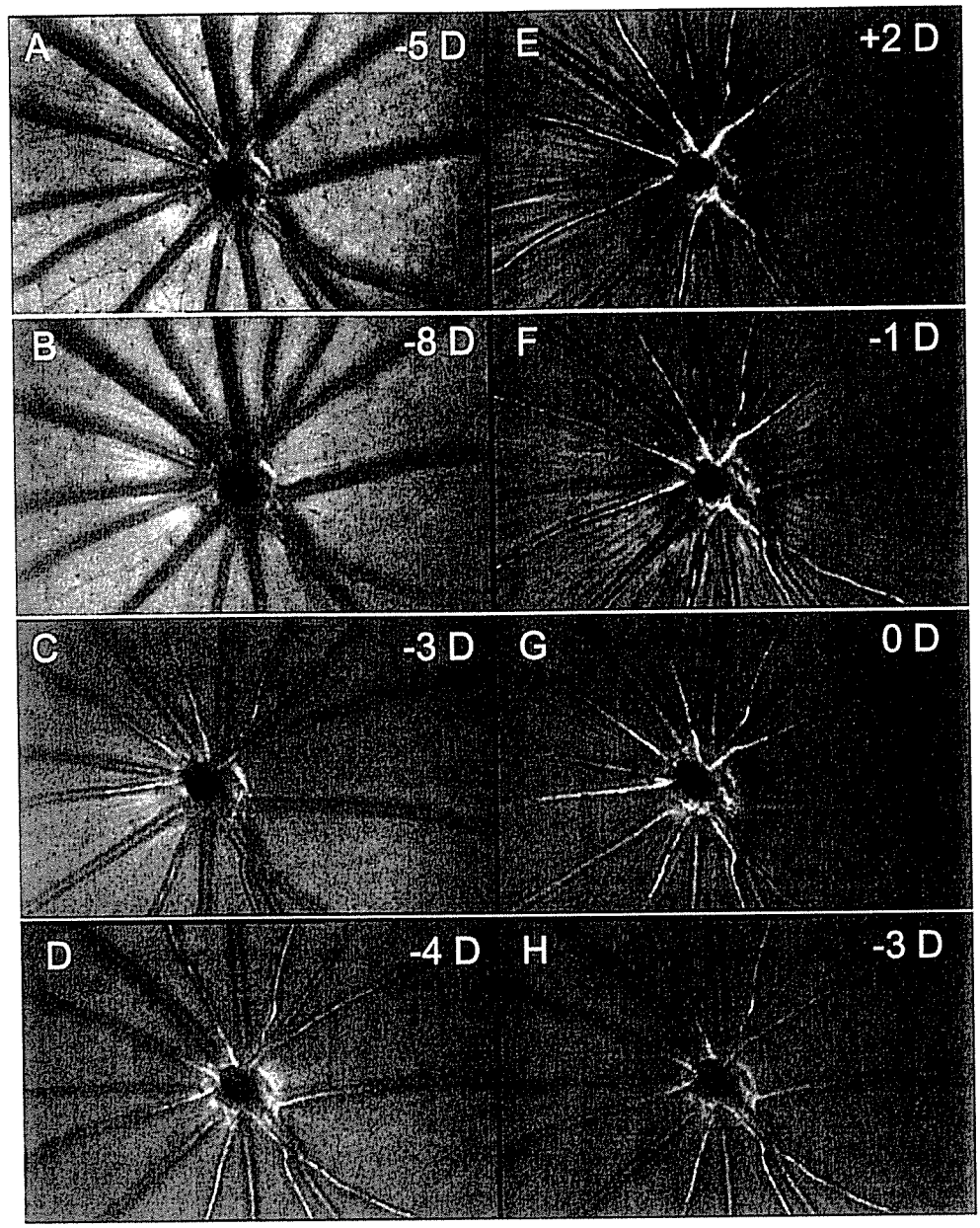

FIGURE 2. RNFL changes over time caused by optic nerve crush. SLO images at baseline (**A**, **E**) and 1 (**B**, **F**), 2 (**C**, **G**), and 4 (**D**, **H**) weeks after axonal injury. (**A**–**D**) Fundus images taken at the lower limit of refractive value for RNFL observation. (**E**–**H**) Fundus images taken at the upper limit of refractive value for RNFL observation. The refractive value of each SLO image is shown at *top right*.

analyzed by one-way ANOVA and post hoc tests. Spearman's rank-order correlation coefficient was calculated to determine the significance of the correlation between ΔF and RNFL thickness measured in retinal sections. $P < 0.05$ was considered statistically significant. Data are expressed as the mean ± SD.

RESULTS

Striations of RNFL radiating from the optic disc were clearly visible in each eye by SLO under argon blue laser illumination when appropriately focused (Fig. 1). The fundus images were sharper, but darker through a C1 than through a C3 confocal aperture (data not shown). After the optic nerve crush, no obvious changes in RNFL reflex were observed 1 week later. However, 2 weeks after the crush, striations of RNFL became uniformly darker and thinner, suggesting diffuse loss of retinal ganglion cell axons. Disappearance of RNFL striations was more evident 4 weeks after the crush (Fig. 2). The RNFL changes after the optic nerve crush were consistent in all 21 rats. In contrast, RNFL appearance of control eyes was unchanged throughout the experimental period.

For the quantitative evaluation of RNFL thickness, the range of refractive values (ΔF) in the SLO setting in which radial striations of RNFL was clearly observed near the optic disc was determined at each time point in both eyes of all 21 rats. The ΔF before and 1, 2, and 4 weeks after the optic nerve crush was 7.1 ± 0.4, 7.2 ± 0.7, 3.4 ± 0.5 and 1.2 ± 0.4 D, respectively (Fig. 3). The ΔF was unchanged 1 week after the crush, but then decreased significantly and progressively after the second week. No significant changes in ΔF were observed in the untreated control eyes during the experimental period.

To determine whether ΔF is a reliable indicator of actual RNFL thickness, the thickness was measured in frozen sections of the retina after the ΔF measurements by SLO (Fig. 4). The RNFL thickness at a location approximately 500 μm temporal from the center of the optic disc in retinal sections before and 1, 2, and 4 weeks after the optic nerve crush was 24.9 ± 2.4, 25.9 ± 3.3, 9.8 ± 1.0, and 3.9 ± 0.2 μm, respectively. The

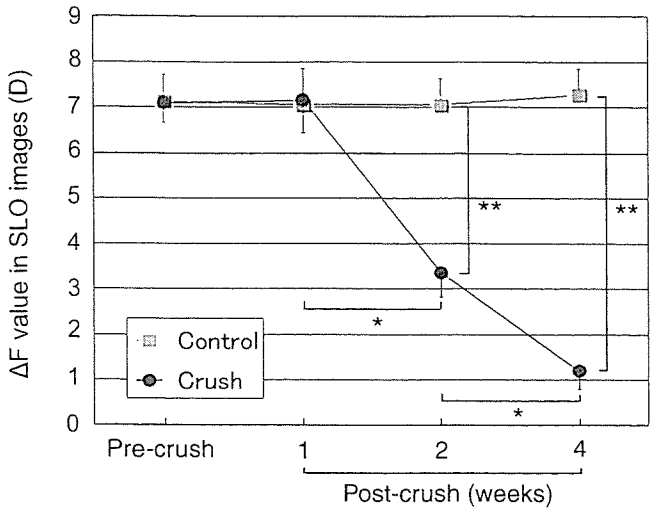

FIGURE 3. Changes of ΔF in SLO images over time caused by the optic nerve crush. Fundus images were recorded using a 1-D step and the range of refractive values (ΔF) where radial striations of RNFL were clearly observed near the optic disc was determined. Data are presented as the mean ± SD (n = 21 each). *P < 0.001 (Friedman test and post hoc tests). **P < 0.001 (Wilcoxon signed-rank test).

thickness was unchanged 1 week after the crush, but then decreased significantly and progressively after the second week. There was a significant positive relationship (r = 0.86, P < 0.001) between ΔF and the histologically determined RNFL thickness (Fig. 5). In contrast, the cell counts in the ganglion cell layer expressed as a percentage of the baseline count (100% ± 6.7%) were 73.6% ± 6.6%, 41.4% ± 2.0%, and 22.8% ± 2.4% at 1, 2, and 4 weeks after optic nerve crush, respectively. This decrease in cell count from baseline was significant 1 week after the crush and progressed further thereafter (P < 0.01).

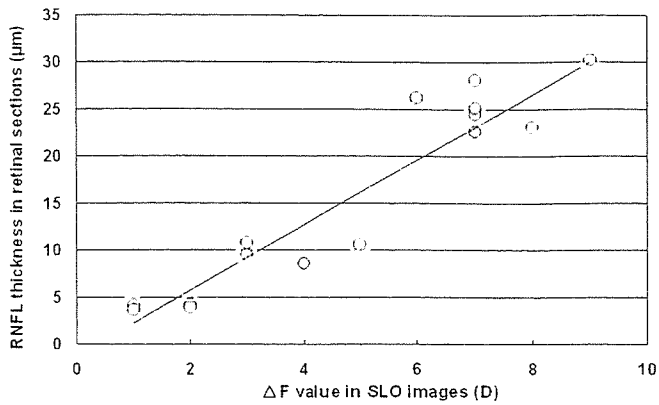

FIGURE 5. Correlation of ΔF and histologically determined RNFL thickness. Spearman's rank-order correlation coefficient analysis shows a significant positive relationship between ΔF and the histologically determined RNFL thickness (r = 0.86, P < 0.001, n = 16).

DISCUSSION

In contrast to the clinical significance of RNFL assessment for diagnosis and management of glaucoma and other optic neuropathies, there have been few reports dealing with the changes of the RNFL or intraretinal axons of retinal ganglion cells in rodent models with optic nerve injuries. An immunohistochemical study showed thick bundles of retinal ganglion cell axons converging toward the optic disc in wholemounts of normal rat retina.[6] The striations radiating from the optic disc in rat retina observed by SLO imaging under argon blue laser illumination seemed quite similar to the intraretinal distribution of retinal ganglion cell axons.[6] Given that the condition used for imaging the rat retina in this study was optimal for RNFL observation of human retina, the radial striations in SLO images were considered to be the reflex from the bundle of retinal ganglion cell axons.

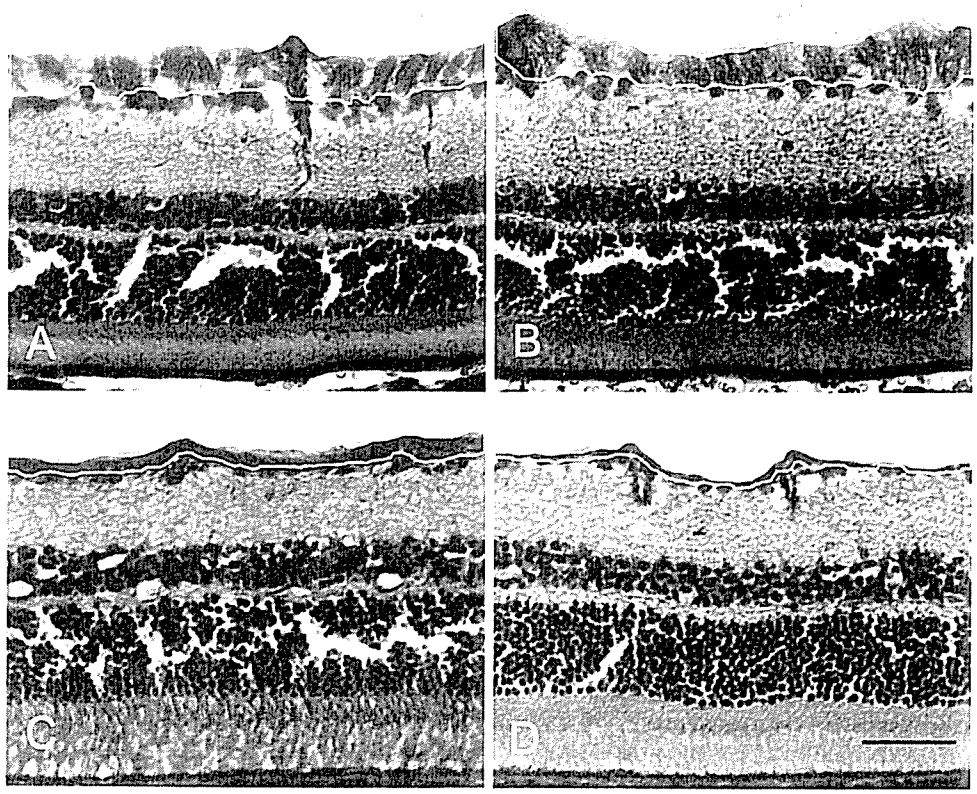

FIGURE 4. Representative photographs of retinal sections showing the changes of RNFL after the optic nerve crush. (A) Baseline and (B) 1, (C) 2, and (D) 4 weeks after axonal injury. *White line* demarcates the area of RNFL in each retinal section. The size of the RNFL area was measured with image-analysis software and the average RNFL thickness of three serial sections was determined. Scale bar, 50 μm.

The clinical usefulness of RNFL evaluation by SLO is limited because SLO evaluation of human RNFL remains qualitative. Other imaging modalities such as optical coherence tomography and nerve fiber layer polarimetry are more suitable for quantitative evaluation of RNFL thickness. However, there have been no reports of in vivo quantitative measurement of RNFL in rodent retina by these methods. The radial striations of RNFL in SLO images appeared to be much stronger in Brown Norway rats than in humans. We used pigmented rats for RNFL evaluation, as visualization of RNFL by argon laser is better in pigmented than in albino rats (data not shown). This better visualization by pigmentation is probably because most of the incident light is absorbed by pigments in the retinal pigment epithelium and the choroid and then reflected light from these tissues is greatly reduced.

We then attempted to evaluate rat RNFL quantitatively by SLO. The smallest setting of the confocal aperture in the SLO used in this study was 1 mm (C1), a setting considerably larger than those in tomographic instruments. Woon et al.[11] measured the axial resolution of this SLO using a C1 confocal aperture in a human model eye and reported that the resolution was 300 μm in a 20° field of view. They used a model eye that consisted of a 16-mm lens and a micrometer mounted mirror. The pixel brightness of the SLO image of the mirror was then plotted against the axial displacement of the mirror. The full-width-at-half-maximum brightness was taken as the axial resolution. Even with this setting, the possibility of optical sectioning and in vivo three-dimensional reconstruction of the human fundus by SLO was reported.[12] Furthermore, considerably improved axial resolution can be achieved with an SLO (Rodenstock). Fitzke et al.[13] reported an optical section of 28 μm with a confocal aperture of 1 mm using a ×8 magnification system for the prototype SLO (Rodenstock).

A similar situation occurs when viewing the rat fundus by SLO. According to data of representative rat[14] and human (Gullstrand's schematic eye) eyes, the axial length of a rat eye is much shorter than that of humans (6.29 vs. 24.00 mm), and the total power of the rat eye is much greater than in humans (300.705 vs. 58.64 D). Therefore, lateral magnification of the rat fundus in SLO images should be approximately five times larger than that of the human fundus. We confirmed that SLO images of the rat fundus were approximately five times larger than images of the human fundus, with the size of the rat and human optic discs (~300 vs. 1500 μm in diameter) being similar in SLO images with the same size field of view. Given that axial magnification is determined by the square of the lateral magnification, the axial magnification of the SLO images of a rat fundus should therefore have been approximately 25 times larger than those of humans in a field of view of the same size. Therefore, when taking SLO images in a 40° field of view, as used in this study, the axial magnification of a rat fundus will be 6.25 times larger than human SLO images in a 20° field of view with the axial resolution of 300 μm.[11] Accordingly, the axial resolution of the rat SLO images would have been approximately 50 μm in this study. Given that the thickness of human and rat retina are similar (typically 250 vs. 170 μm[14]), optical sectioning of a rat fundus by an SLO (Rodenstock) should be superior to that achieved in humans.

As for the 1-D step of the ametropic corrector to evaluate RNFL thickness in this study, adding 1 D to the ametropic correction moves the plane of focus approximately 0.3 mm in the direction of the vitreous in the human eye, because adding 1 D to the total power of the human eye makes the posterior focal length approximately 0.3 mm shorter in Gullstrand's schematic eye. In contrast, the posterior focal length in a rat eye[14] is calculated to be approximately 10 μm shorter when adding 1 D to the total power of the rat eye. Thus, a 1-D step in the ametropic correction moves the focal plane approximately 10 μm, a step that is not too wide for measuring RNFL thickness ($\leq$25 μm) with an axial resolution of approximately 50 μm.

In agreement with the theoretical consideration of the ability of the SLO for optical sectioning of a rat fundus, the focus measurement of rat RNFL (ΔF) using this technique was performed successfully with good intra- and interobserver reproducibility using a 1-mm confocal aperture.

In the next step, we compared the ΔF and the actual RNFL thickness in histologic sections to verify that ΔF is a reliable indicator of RNFL thickness. Although RNFL thickness may vary at different distances from the optic disc, we consistently measured the RNFL thickness at a location approximately 500 μm temporal from the center of the optic disc. At this location, the visibility of radial striations of RNFL in SLO images was suitable for determination of the ΔF value and also the RNFL was thick enough for measuring the changes in retinal sections.

Given a nominal 1-D step of the ametropic corrector corresponding to approximately 10-μm movement of the focal plane and the axial resolution of approximately 50 μm (full-width-at-half-maximum brightness) in SLO images of rat fundus, the ΔF of approximately 7 D for the 25-μm thickness of normal rat RNFL is reasonable. In contrast, ΔF was approximately 1 D for <5 μm of RNFL thickness in the retina 4 weeks after the optic nerve crush, although it should have been $\geq$5 D, theoretically. This discrepancy may be explained as follows. The half-maximum brightness of the normal rat RNFL reflex in SLO images may be similar to the threshold of seeing the reflex. However, for thinner RNFL, the visibility became lower, and then stricter focusing (i.e., smaller ΔF values) may have been needed to see the reflex.

The significant positive relationship between ΔF and the histologically determined RNFL thickness indicates that ΔF is a reliable indicator of actual RNFL thickness and, thus, quantitative analysis of rat RNFL can be performed by SLO.

The RNFL thickness was unchanged until the first week after the optic nerve crush in SLO images and retinal sections. Furthermore, we did not notice any qualitative changes of the RNFL reflex in either SLO images or intraretinal axon bundles in histologic sections between baseline and 1 week after the crush. As for the loss of retinal ganglion cell bodies after the optic nerve crush or axotomy, the time course and magnitude of cell death depends on the severity of the injury[15,16] and the distance of the injury site from the ganglion cell bodies.[17] When the optic nerve is damaged intraorbitally, ganglion cell death starts several days after injury,[18] reaches 30% to 50% 1 week after,[19-21] and progresses further thereafter. In this study, as an index of ganglion cell loss, we counted the number of cells in the ganglion cell layer in the retinal sections used for measuring RNFL thickness and found that the decrease in cell counts was significant 1 week after the crush. Thus, the result of this study suggests that loss of cell bodies may precede the loss of intraretinal axons of retinal ganglion cells after the optic nerve crush. The implication of dissociation between the time course of changes in intraretinal axons and cell bodies is currently unknown. Given that retinal ganglion cells of the adult rat die through apoptosis when axotomized,[22] the clearance processes for apoptotic cell bodies may differ from those for intraretinal axons. Further studies are needed to examine this hypothesis.

In conclusion, SLO is a useful and valuable tool for in vivo imaging and quantification of rat RNFL. Evaluation of rat RNFL by SLO will be informative not only in optic nerve crush models but also in other models of optic nerve damage for studying the pathology of optic neuropathy including glaucoma and for developing new therapies.

References

1. Blumenthal EZ, Weinreb RN. Assessment of the retinal nerve fiber layer in clinical trials of glaucoma neuroprotection. *Surv Ophthalmol.* 2001;45:S305-S312.
2. Miglior S, Rossetti L, Brigatti L, Bujtar E, Orzalesi N. Reproducibility of retinal nerve fiber layer evaluation by dynamics scanning laser ophthalmoscopy. *Am J Ophthalmol.* 1994;118:16-23.
3. Nishiwaki H, Ogura Y, Kimura H, Kiryu J, Honda Y. Quantitative evaluation of leukocyte dynamics in retinal microcirculation. *Invest Ophthalmol Vis Sci.* 1995;36:123-130.
4. Goldblum D, Mittag T. Prospects for relevant glaucoma models with retinal ganglion cell damage in the rodent eye. *Vision Res.* 2002;42:471-478.
5. Allcutt D, Berry M, Sievers J. A quantitative comparison of the reactions of retinal ganglion cells to optic nerve crush in neonatal and adult mice. *Brain Res.* 1984;318:219-230.
6. Villegas-Perez MP, Vidal-Sanz M, Bray GM, Aguayo AJ. Influences of peripheral nerve grafts on the survival and regrowth of axotomized retinal ganglion cells in adult rats. *J Neurosci.* 1988;8:265-280.
7. Chauhan BC, Pan J, Archibald ML, LeVatte TL, Kelly ME, Tremblay F. Effect of intraocular pressure on optic disc topography, electroretinography, and axonal loss in a chronic pressure-induced rat model of optic nerve damage. *Invest Ophthalmol Vis Sci.* 2002; 43:2969-2976.
8. Mabuchi F, Aihara M, Mackey MR, Lindsey JD, Weinreb RN. Optic nerve damage in experimental mouse ocular hypertension. *Invest Ophthalmol Vis Sci.* 2003;44:4321-4330.
9. Allcutt D, Berry M, Sievers J. A qualitative comparison of the reactions of retinal ganglion cell axons to optic nerve crush in neonatal and adult mice. *Brain Res.* 1984;318:231-240.
10. Sugiyama K, Gu ZB, Kawase C, Yamamoto T, Kitazawa Y. Optic nerve and peripapillary choroidal microvasculature of the rat eye. *Invest Ophthalmol Vis Sci.* 1999;40:3084-3090.
11. Woon WH, Fitzke FW, Bird AC, Marshall J. Confocal imaging of the fundus using a scanning laser ophthalmoscope. *Br J Ophthalmol.* 1992;76:470-474.
12. Fitzke FW, Masters BR. Three-dimensional visualization of confocal sections of *in vivo* human fundus and optic nerve. *Curr Eye Res.* 1993;12:1015-1018.
13. Fitzke FW, Woon H, Timberlake G, Robinson L, Marshall J, Bird AC. Optical modifications to a scanning laser ophthalmoscope for high magnification, narrow optical section imaging. *Lasers Light Ophthalmol.* 1991;4:7-14.
14. Hughes A. A schematic eye for the rat. *Vision Res.* 1979;19:569-588.
15. Berkelaar M, Clarke DB, Wang YC, Bray GM, Aguayo AJ. Axotomy results in delayed death and apoptosis of retinal ganglion cells in adult rats. *J Neurosci.* 1994;14:4368-4374.
16. Gellrich NC, Schimming R, Zerfowski M, Eysel UT. Quantification of histological changes after calibrated crush of the intraorbital optic nerve in rats. *Br J Ophthalmol.* 2002;86:233-237.
17. Villegas-Perez MP, Vidal-Sanz M, Rasminsky M, Bray GM, Aguayo AJ. Rapid and protracted phases of retinal ganglion cell loss follow axotomy in the optic nerve of adult rats. *J Neurobiol.* 1993;24:23-36.
18. Levkovitch-Verbin H, Quigley HA, Martin KRG, Zack DJ, Pease ME, Valenta DF. A model to study differences between primary and secondary degeneration of retinal ganglion cells in rats by partial optic nerve transaction. *Invest Ophthalmol Vis Sci.* 2003;44: 3388-3393.
19. Barron KD, Dentinger MP, Krohel G, Easton SK, Mankes R. Qualitative and quantitative ultrastructural observations on retinal ganglion cell layer of rat after intraorbital optic nerve crush. *J Neurocytol.* 1986;15:345-362.
20. Mansour-Robaey S, Clarke DB, Wang YC, Bray GM, Aguayo AJ. Effects of ocular injury and administration of brain-derived neurotrophic factor on survival and regrowth of axotomized retinal ganglion cells. *Proc Natl Acad Sci USA.* 1994;91:1632-1636.
21. Selles-Navarro I, Ellesam B, Fajardo R. Retinal ganglion cell and nonneural cell responses to a microcrush lesion of adult rat optic nerve. *Exp Neurol.* 2001;167:282-289.
22. Garcia-Valenzuela E, Gorczyca W, Darzynkiewicz Z, Sharma SC. Apoptosis in adult retinal ganglion cells after axotomy. *J Neurobiol.* 1994;25:431-438.

In Vivo Imaging and Counting of Rat Retinal Ganglion Cells Using a Scanning Laser Ophthalmoscope

Tomomi Higashide, Ichiro Kawaguchi, Shinji Ohkubo, Hisashi Takeda, and Kazuhisa Sugiyama

Purpose. To determine whether a scanning laser ophthalmoscope (SLO) is useful for in vivo imaging and counting of rat retinal ganglion cells (RGCs).

Methods. RGCs of Brown Norway rats were retrogradely labeled bilaterally with the fluorescent dye 4-(4-(dihexadecylamino)styryl)-*N*-methylpyridinium iodine (DiA). The unilateral optic nerve was crushed intraorbitally with a clip. RGCs were imaged in vivo with an SLO with an argon blue laser (488 nm) and optical filter sets for fluorescein angiography, before and 1, 2, and 4 weeks after the crush. Fluorescent cells were also counted in retinal flatmounts at baseline and 1, 2, and 4 weeks after the crush. An image overlay analysis was performed to check cell positions in the SLO images over time. Lectin histochemical analysis was performed to determine the relationship of microglia to the newly emerged DiA fluorescence detected by image overlay analysis after the optic nerve crush.

Results. Fluorescent RGCs were visible in vivo with an SLO. RGC survival decreased gradually after the crush. In the retina after the optic nerve crush, newly emerged DiA fluorescence detected by image overlay analysis corresponded to fluorescent cells morphologically different from RGCs in the retinal flatmount and was colocalized mostly with lectin-stained microglial processes. RGC counts by SLO were comparable to those in retinal flatmounts.

Conclusions. The SLO is useful for in vivo imaging of rat RGCs and therefore may be a valuable tool for monitoring RGC changes over time in various rat models of RGC damage. (*Invest Ophthalmol Vis Sci.* 2006;47:2943–2950) DOI:10.1167/iovs.05-0708

Ocular hypertension, ischemia-reperfusion, and optic nerve crush rodent models have helped elucidate the pathophysiology of glaucoma and other optic neuropathies.[1] In these models, the number of retinal ganglion cells (RGCs) is usually counted in retinal flatmounts that are prepared after labeling of RGCs, then the changes of RGCs are evaluated by comparing the equivalent retinal positions in experimental and control eyes.[2–4] However, inconsistency of staining efficacy or inherent variability of RGC density[5] prevents detection of small differences in RGC survival between experimental and control eyes.

Examination of RGC changes in vivo over time may overcome this drawback. Only a few papers have reported successful imaging of rat RGCs in vivo with a confocal laser scanning microscope,[6] a fluorescence microscope,[7] or conventional infrared fundus photography.[8] Recently, in vivo imaging of RGC apoptosis using a confocal laser scanning microscope has been reported.[9] However, imaging techniques using a confocal laser scanning microscope or a fluorescence microscope have not been widely adopted because of the limited availability of the equipment and the necessary special modifications of the microscope. Counts of RGCs made with infrared fundus photography have not been published. Therefore, a new methodology for in vivo imaging of RGCs is needed.

The scanning laser ophthalmoscope (SLO) is widely used in fluorescein and indocyanine green angiography to examine human retinal diseases. Furthermore, the SLO has been reported to be useful for evaluation of the retinal nerve fiber layer and the optic disc of human glaucomatous eyes.[10,11] The SLO can also be used for imaging rat retinas to study retinal microcirculation.[12] In this study, we wanted to determine whether the SLO is useful for in vivo imaging and counting of rat RGCs by using the optic nerve crush model.

Methods

Animals

Male Brown Norway rats, 12 weeks of age and weighing 200 to 250 g, were used. Six rats (group 1) were used for in vivo RGC imaging by SLO over time (before and 1, 2, and 4 weeks after unilateral optic nerve crush) and to compare the SLO images and retinal flatmount images at 4 weeks after optic nerve crush. The comparison of both images in the nonsurgical eyes served as baseline data. In addition, 12 rats (group 2) were used to compare the images of SLO and retinal flatmounts at 1 and 2 weeks after optic nerve crush (6 rats for each time point). Furthermore, three rats (group 3) for each time point (baseline and 1, 2, and 4 weeks after optic nerve crush) were used for the histochemical analyses of microglia.

All animals were treated in accordance with the ARVO Statement for the Use of Animals in Ophthalmic and Vision Research. Experiments were conducted on rats anesthetized by intraperitoneal injection of pentobarbital sodium (65 mg/kg).

Retrograde Fluorescent Staining of RGCs

Retrograde staining of RGCs of both eyes was achieved by injecting a fluorescent dye into the superior colliculus bilaterally. Rats were placed in a stereotactic apparatus (Narishige Co. Ltd., Tokyo, Japan), and the skin of the skull was incised. The brain surface was exposed by perforating the parietal bone with a dental drill to facilitate dye injection. A fluorescent dye, 4-(4-(dihexadecylamino)styryl)-*N*-methylpyridinium iodine (DiA; Invitrogen, Eugene, OR), was dissolved in dimethylformamide (Sigma-Aldrich, St. Louis, MO) at a concentration of 10 μg/mL. The dye solution (2.0 μL) was injected at a point 5.5 mm caudal to the bregma and 1.5 mm lateral to the midline on both sides to a depth of 4.5 mm from the surface of the skull, in accordance with the results of preliminary experiments to identify the position of the superior colliculus.

From the Department of Ophthalmology, Kanazawa University Graduate School of Medical Science, Kanazawa, Japan.

Supported by a Grant-in-Aid for Scientific Research from the Ministry of Education, Science, and Culture, Japan.

Submitted for publication June 7, 2005; revised October 27, 2005, and February 23, 2006; accepted May 15, 2006.

Disclosure: **T. Higashide**, None; **I. Kawaguchi**, None; **S. Ohkubo**, None; **H. Takeda**, None; **K. Sugiyama**, None

The publication costs of this article were defrayed in part by page charge payment. This article must therefore be marked "*advertisement*" in accordance with 18 U.S.C. §1734 solely to indicate this fact.

Corresponding author: Tomomi Higashide, Department of Ophthalmology, Kanazawa University Graduate School of Medical Science, 13-1 Takara-machi, Kanazawa, Ishikawa 9208641, Japan; eyetomo@kenroku.kanazawa-u.ac.jp.

In Vivo Imaging of RGCs with the SLO

The eyes were dilated with 0.5% tropicamide and 0.5% phenylephrine hydrochloride eye drops (Santen Pharmaceuticals, Osaka, Japan). To preserve corneal clarity throughout the experiment, we placed a custom-made contact lens with a radius of curvature of 2.75 mm and a diameter of 5.0 mm (Kyoto Contact Lens, Kyoto, Japan) on the cornea after topical anesthesia with 0.4% oxybuprocaine hydrochloride eye drops (Santen Pharmaceuticals). A rat was placed on a heating pad (Deltaphase Isothermal Pad; Braintree Scientific, Inc., Braintree, MA), and its head was gently held manually to keep the eye in position for viewing the fundus with an SLO (SLO 101; Rodenstock Instruments, Munich, Germany). Under illumination with an argon blue laser (488 nm), we focused on the retinal surface by changing the refractive values in the SLO setting, visualizing fluorescent RGCs through the optical filter sets for fluorescein angiography. Dynamic fundus images with a field angle of 40° were recorded in the center of the fundus and also in the midperipheral area. The SLO images were digitized by an analog-to-digital video converter (Canopus ADVC-300; Canopus Co., Ltd., Kobe, Japan) and saved as DV-AVI files on a computer (VAIO VGC-RA50S; Sony Corp., Tokyo, Japan), running commercial computer software (DV GatePlus; Sony Corp.). In vivo images of RGCs were obtained before and 1, 2, and 4 weeks after optic nerve crush.

Intraorbital Optic Nerve Crush

Intraorbital optic nerve crush was performed 2 months after the retrograde staining of RGCs because we observed a gradual increase in the intensity and the area of RGC staining for up to 2 months after dye injection (data not shown). The conjunctiva of the right eye was incised in the superotemporal quadrant to expose the optic nerve by careful blunt dissection under an operating microscope. The optic nerve was crushed 2 mm behind the globe for 30 seconds with a 60-g clip (Micro Vascular Clip; Roboz Surgical Instrument Co., Gaithersburg, MD). Special care was taken not to damage the blood supply to the eye. The fundus was monitored by indirect ophthalmoscopy, and immediate recovery of retinal blood supply was observed in each eye after removal of the clip. The left eye had no operation.

Retinal Flatmounts

In group 1 rats, both eyes were subjected to retinal flatmount preparation 4 weeks after the optic nerve crush. In group 2 and 3 rats, the retinal flatmounts were prepared from the right eye.

Immediately after in vivo imaging of RGCs, the eyes were enucleated after administration of an overdose of anesthesia by an intraperitoneal injection of pentobarbital sodium. The anterior segments were removed, and the resultant posterior eye cups were fixed in 4% paraformaldehyde and 0.1 M phosphate-buffered saline (PBS) for 1 hour at room temperature. After six radial cuts were made in the periphery of the eye cup, the retina was carefully separated from the retinal pigment epithelium. A small marking cut was placed in the peripheral corner of the superior retinal portion for the correct identification of the retinal orientation. The retina was then flatmounted on a glass slide, covered with an antifade mounting solution (Vectashield; Vector Laboratories, Burlingame, CA) and glass coverslip, and kept in the dark at 4°C until microscopic observation.

RGCs in the retinal flatmounts were examined with a fluorescence microscope (Nikon Eclipse TE300; Nikon Corp., Kanagawa, Japan) equipped with a filter set (excitation filter 450 to 490 nm; barrier filter 520 nm; B-2A; Nikon) and 10× objective. RGC images were recorded as JPEG files with a digital cooled charge-coupled device camera (DS-5Mc-L1; Nikon) and were stored on a computer (Dimension 8300; Dell Inc., Round Rock, TX).

Image Analysis for Cell Counting

A retinal area 0.5 to 1.5 mm from the center of the optic disc, where cells were intensely stained and were well focused in SLO images throughout the experimental period, was selected for each eye. Still images of the selected retinal area were created from the DV-AVI files of dynamic SLO images by using video-editing software (Premiere 6.5; Adobe Systems Inc., Mountain View, CA). The identical retinal area of the same eye was determined in SLO images obtained at different times and also in the flatmount images by using image-editing software (Photoshop, ver. 6.0; Adobe Systems Inc.). The number of labeled cells in the selected area of each image was counted manually in a masked fashion by the same investigator. Small spots of punctate fluorescence observed in the flatmounted images after the optic nerve crush were not included in the cell count because they represented cell debris of dead RGCs (see Fig. 2J, arrows).[13] When counting RGCs only, we applied the morphologic criteria for discriminating non-RGC cells from RGCs.[13,14] Cells with irregular shape, intense DiA staining, and smaller or larger size than typical RGCs (see Fig. 5D) were considered to be non-RGC cells such as microglia (see Fig. 5, arrows in 5H, 5L, 5P). The size of the retinal area for RGC counting was measured in the flatmount images using image-analysis software (Image-Pro Express 4.0; Media Cybernetics, Inc., Silver Spring, MD), and the density of labeled cells in each image was calculated.

Image Overlay Analysis

To distinguish RGCs from other types of cells, which presumably were microglial cells that became fluorescent by phagocytosis of cell debris of RGCs after optic nerve crush, an image overlay analysis was performed. The cell positions in the SLO images taken after optic nerve crush were compared with those at baseline in the analysis. Because RGCs are not mobile and are stably labeled by retrograde transport of DiA 2 months after dye injection, fluorescent cells that have emerged in a location where no fluorescence was observed before should be other types of cells. With the image analysis software (Photoshop; Adobe Systems, Inc.), the SLO images recorded before optic nerve crush had their brightness inverted and were overlaid as a 50% opaque layer onto the SLO images of the same retinal area taken after axonal injury. Theoretically, if the precrush image were identical with the postcrush image, the composite image, which is produced by the overlay with perfect alignment of the two images, would become homogeneously gray. Slight misalignment of identical spots in the two images produces a shadowing effect around the spots. In contrast, fluorescent spots that disappeared or emerged after the crush should appear as black or white spots in the composite images. The image

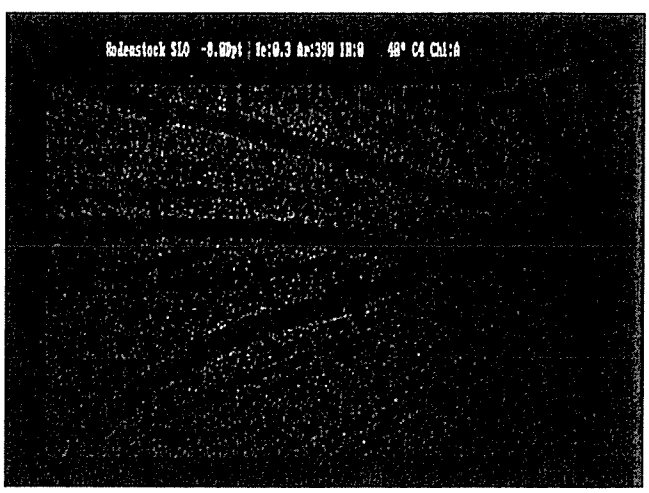

FIGURE 1. Representative SLO image of normal rat retina showing retinal ganglion cells (RGCs) retrogradely labeled with DiA. SLO imaging was performed with an argon blue laser (488 nm) and optical filter sets for fluorescein angiography. Labeled RGCs are visible as *white* spots.

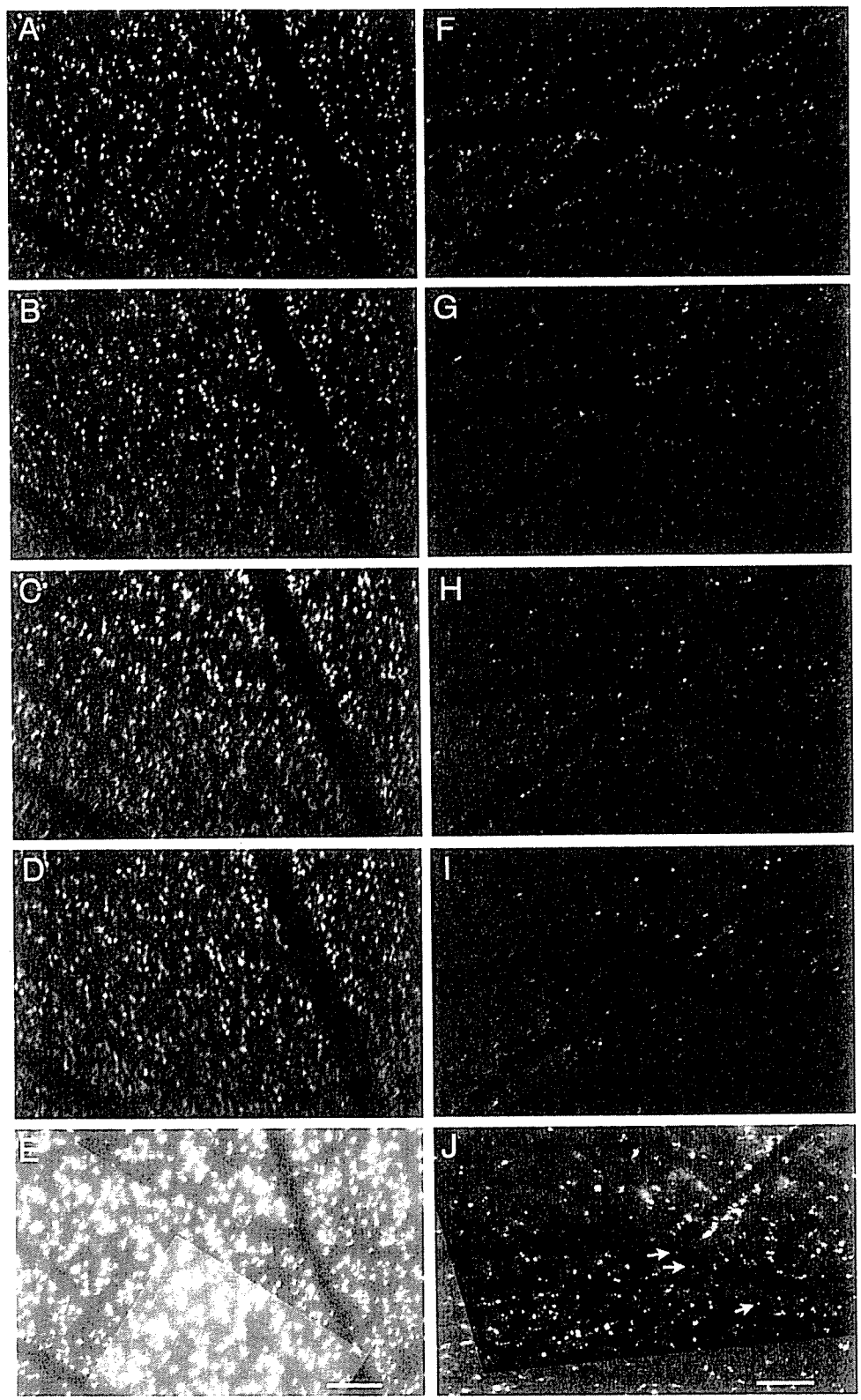

FIGURE 2. Representative photographs showing the changes of DiA-labeled cells in the same retinal area of control (**A–E**) and experimental (**F–J**) eyes. (**A–D**, **F–I**) SLO images; (**E**, **J**) flatmount images. The optic nerve of the right eye was crushed intraorbitally with a clip. The left eye served as the untreated control. SLO imaging of the same retinal area of control and experimental eyes was performed before (**A**, **F**) and at 1 (**B**, **G**), 2 (**C**, **H**), and 4 (**D**, **I**) weeks after axonal injury. Retinal flatmounts of control (**E**) and experimental (**J**) eyes were prepared after the SLO imaging at postcrush week 4, and the same retinal areas of SLO images were examined by fluorescence microscopy. *Arrows*: small spots of punctate fluorescence representing cell debris of dead RGCs. Scale bar, 100 μm.

overlay system was used in the rats in group 1 (for control and 4 weeks after the crush) and group 2 (for 1 and 2 weeks after the crush). The composite SLO images were compared with the identical retinal area in the flatmounts. RGC counts in SLO images were determined by subtracting the number of newly emerged fluorescent cells from total cell counts.

Histochemical Analysis of Microglia

For the group 3 rats, SLO imaging of RGCs was performed at baseline and at the time when the retinal flatmounts were to be prepared. After obtaining images of DiA-labeled RGCs with an SLO in vivo and with a fluorescence microscope (Axioplan 2; Carl Zeiss GmbH, Jena, Ger-

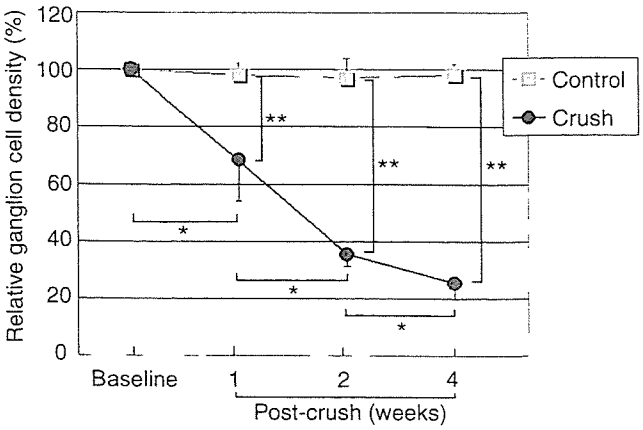

FIGURE 3. The DiA-labeled cell density after optic nerve crush determined by SLO. The relative density of labeled cells in selected retinal areas of an SLO image at each time point was determined in each eye, with labeled cell density of the SLO image taken at baseline being 100%, and the results were averaged. Data are presented as the mean ± SD (n = 6 each). *$P < 0.01$ (Wilcoxon signed rank test), **$P < 0.01$ (Wilcoxon rank sum test).

many) with a filter set (equivalent to B-2A; Nikon) in the flatmounted retina, we performed histochemical staining of microglia[15] in the flatmounted retina. The glass coverslip covering the retinal flatmounts was carefully removed. The retina was floated in PBS, flatmounted on a nylon membrane (Hybond-N+; GE Healthcare, Piscataway, NJ), and blocked with 0.5% bovine serum albumin in PBS and 1.0% Triton X-100 at room temperature for 1 hour. The retina was then incubated with 20 μg/mL of biotin-conjugated isolectin B4 from *Griffonia simplicifolia* (Sigma-Aldrich, Inc.) in PBS with 0.5% bovine serum albumin and 0.5% Triton X-100 at 4°C overnight. After it was washed in PBS, the retina was treated with 10 μg/mL of Alexa Fluor 350-conjugated avidin (NeutrAvidin; Invitrogen) in PBS with 0.5% bovine serum albumin and 0.1% Triton X-100 at room temperature for 2 hours. The retina was then washed in PBS, carefully peeled from the nylon membrane, flatmounted on a glass slide, and covered with antifade medium (Vectashield; Vector Laboratories) and a glass coverslip. Fluorescence of Alexa Fluor 350 labeling was examined using a fluorescence microscope (Axioplan; Carl Zeiss GmbH) with an appropriate filter set for the dye. The cell density of the microglia was measured at four retinal locations (500 × 500 μm^2 each, 1–1.5 mm from the center of the optic disc) per eye and averaged.

Statistical Analysis

The relative density of labeled cells in the selected retinal area of an SLO image at each time point or of the flatmount image was determined for each eye with the labeled cell density of the SLO image taken before the optic nerve crush being 100%. Differences in cell densities were statistically analyzed by the Wilcoxon rank sum test for comparison between control and crushed eyes and by the Wilcoxon signed rank test for comparison of SLO images taken at different time points and of cell densities between SLO and flatmount images. For the comparison of image overlay analysis and retinal flatmounts, differences in RGC counts by SLO and those in retinal flatmounts were also examined by the Wilcoxon signed rank test. One-way ANOVA tests and post hoc tests were used to assess changes of microglial cell densities caused by optic nerve crush. $P < 0.05$ was considered statistically significant. Data are expressed as the mean ± SD.

RESULTS

Fluorescent RGCs stained with DiA were visible in vivo with an SLO with argon blue laser illumination and the optical filter sets for fluorescein angiography (Fig. 1). Although the retinal area that can be viewed in a single SLO frame was limited, it was not difficult to obtain a retinal image of a desired area by aligning the direction of the rat eye manually. The entire image of an SLO frame could not be focused well simultaneously. However, at least 0.1 mm^2 of retinal area could be focused well simultaneously in an SLO frame. The retinal area used for cell counting in retinas of group 1 in the flatmount preparation was 0.30 ± 0.15 mm^2 (n = 12). The baseline labeled cell density (cell number/retinal area) of the selected retinal areas in both eyes of group 1 rats was 1967 ± 377 cells/mm^2 (n = 12).

After the optic nerve crush, a decrease in fluorescent cells in selected retinal areas of the SLO image was significant at 1 week and progressed at 2 and 4 weeks (Figs. 2, 3). The number of labeled cells in the untreated control eyes remained stable during the experimental period (Figs. 2, 3). To evaluate the validity of cell counts in the SLO images, the number of labeled cells was also determined in retinal flatmounts. The relative density of DiA-labeled cells in SLO images (with that in retinal flatmounts being 100%) was 101.5% ± 9.9%, 98.2% ± 4.8%, 91.3% ± 4.4%, and 99.6% ± 12.0% at baseline and 1, 2, and 4 weeks after optic nerve crush, respectively. Cell counts by SLO were not significantly different from those in retinal flatmounts. However, details of cell structure were less clear in SLO images than in flatmount images (Fig. 2). Furthermore, most of the punctate fluorescence, which we considered to be cell debris of dead RGCs, observed in the flatmount images of postcrush retina was not clearly visible with the SLO (Fig. 2, arrows). Thus, the resolution and sensitivity of fluorescence in SLO images were lower than those in flatmount images.

To identify non-RGC cells which became fluorescent after the optic nerve crush, we performed an image overlay analysis. The overlay composite images of control retinas showed few black or white spots, indicating that few deaths followed by phagocytosis of RGCs occurred in the control retinas during the experimental period (Fig. 4). In contrast, a significant number of black and white spots appeared in the composite images of postcrush retina. The position of white spots changed over time, reflecting the movement of the cells (Fig. 4). Thus, fluorescent spots in SLO images of postcrush retina (Fig. 2) consisted of both surviving RGCs and emerging non-RGC cells.

By comparing the composite SLO images and retinal flatmounts, we determined that the newly emerged fluorescent spots in the SLO images after the optic nerve crush corresponded with fluorescent cells with shapes and sizes different from RGCs in retinal flatmounts (Fig. 5). Therefore, we determined RGC counts in SLO images by subtracting the number of newly emerged fluorescent cells from total cells. The results were compared with RGC counts by retinal flatmounts with application of morphologic criteria[13,14] to discriminate non-RGC cells from RGCs. There were no significant differences between RGC counts by SLO and those by retinal flatmounts in control and postcrush retinas (Fig. 6).

To determine the relationship of microglia to the newly emerged DiA fluorescence after the optic nerve crush, we stained microglia in the retinal flatmounts with isolectin B4 after taking images of DiA fluorescence in SLO and retinal flatmounts. The counts of lectin-labeled microglial cell bodies were 28.3 ± 1.5, 71.3 ± 2.5, 115.3 ± 13.3, and 66.0 ± 10.4/mm^2 at baseline and 1, 2, and 4 weeks after optic nerve crush, respectively (Fig. 7). In agreement with a previous report,[16] optic nerve crush significantly increased the number of microglia, which peaked 2 weeks after the crush. Furthermore, a point-by-point comparison of the overlaid composite images of SLO and lectin-stained retinal flatmounts showed that newly emerged fluorescent spots in SLO images colocalized mostly with microglial processes and occasionally in the vicin-

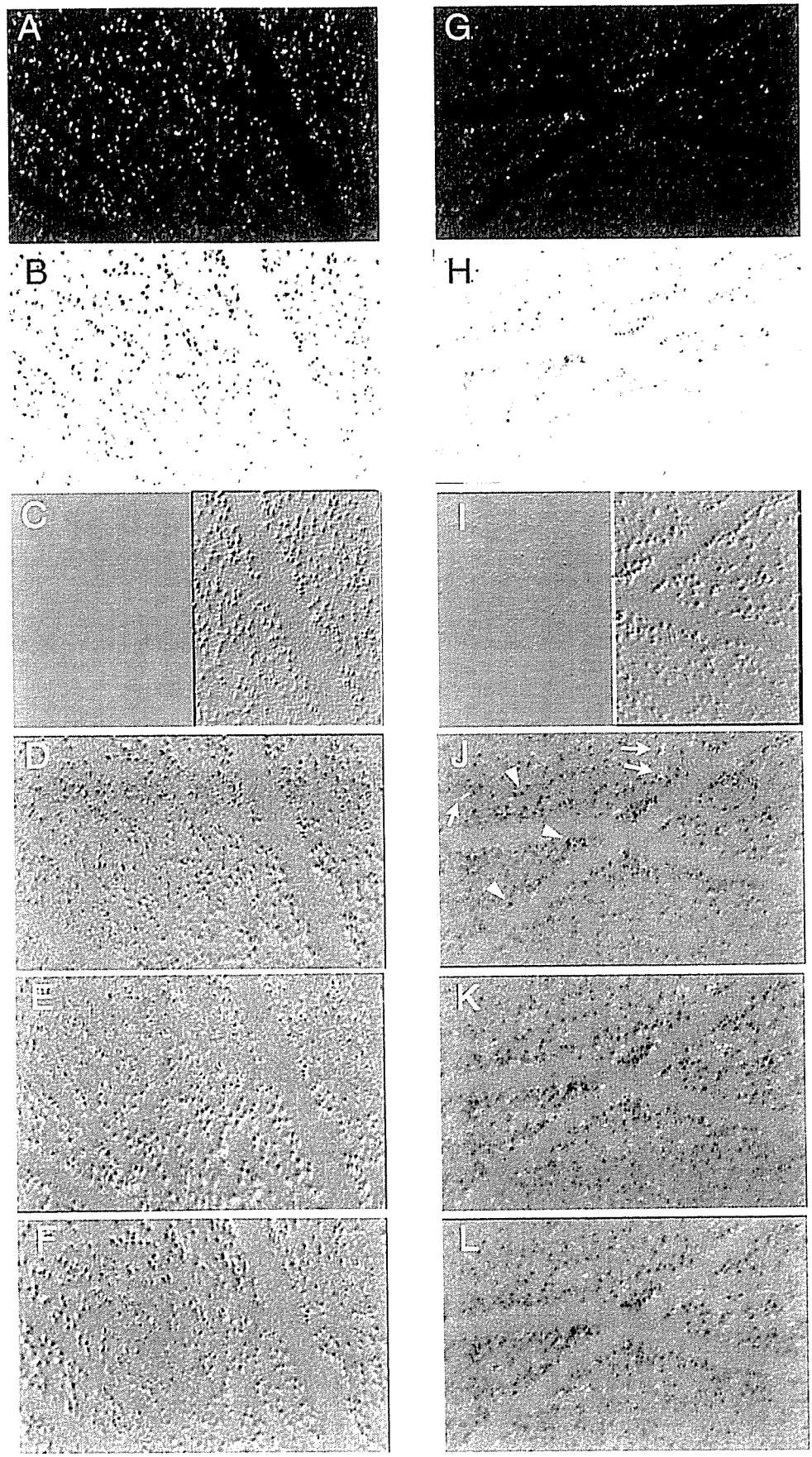

FIGURE 4. Image overlay analysis of SLO images in control (**A**–**F**) and experimental (**G**–**L**) eyes. The SLO image recorded before optic nerve crush (**A**, **G**) had its brightness inverted (**B**, **H**) and was overlaid as a 50% opaque layer, onto the SLO image of the same retinal area taken before (**C**, **I**) and 1 (**D**, **J**), 2 (**E**, **K**), and 4 (**F**, **L**) weeks after axonal injury. Although the composite image of the two identical images became homogeneously gray when they were perfectly aligned (**C**, **I**, *left* half), a shadowing effect around the spots appeared when the spots were slightly misaligned (**C**, **I**, *right* half). Fluorescent spots that disappeared or emerged in the second image should appear as *black* or *white* spots in the composite image, respectively. In control retina, few *black* and *white* spots were observed, aside from the shadowing effect (**D**–**F**). Postcrush retina showed many spots, indicating disappearing RGCs (*black*) and emerging *white* non-RGC cells (**J**–**L**). The position of *white* spots changed over time, reflecting the movement of the cells. *Arrowheads* and *arrows*: examples of *black* and *white* spots, respectively.

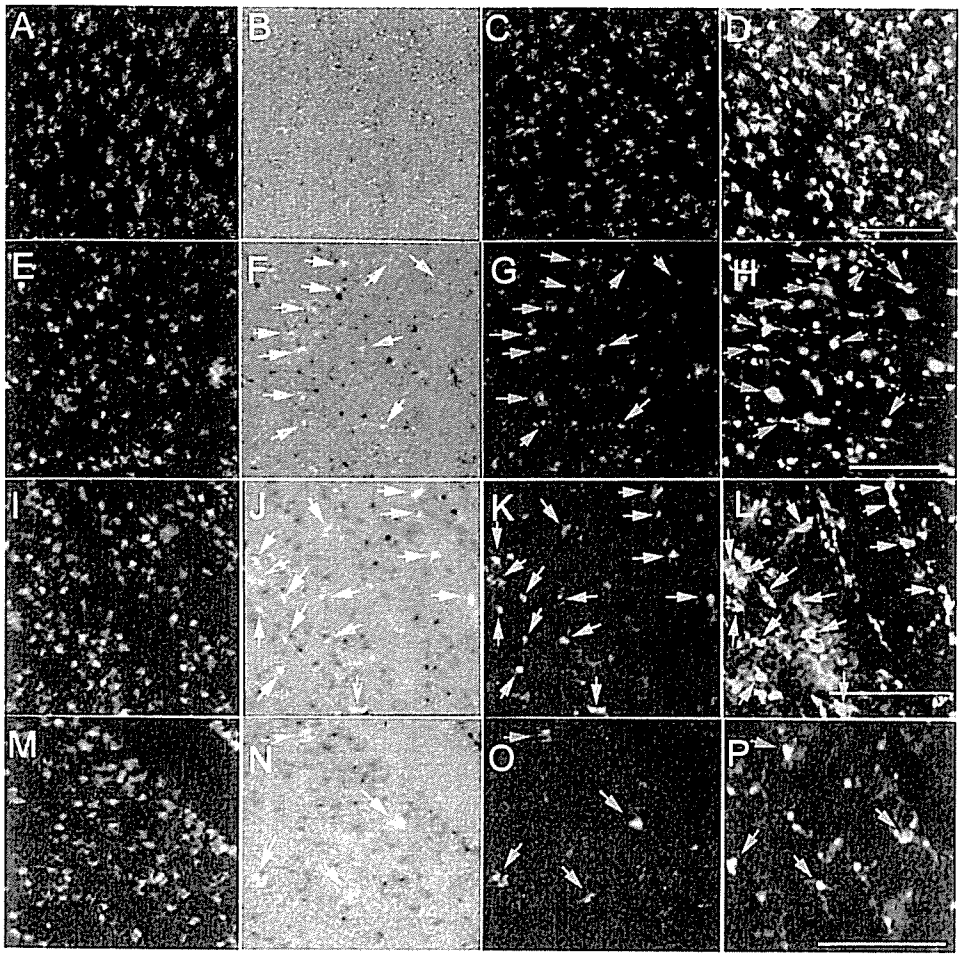

FIGURE 5. Comparison of SLO image overlay system and retinal flatmount in control (**A–D**) and postcrush (1, **E–H**; 2, **I–L**; and 4, **M–P** weeks) retinas. (**A**, **E**, **I**, **M**) baseline SLO images; (**B**, **F**, **J**, **N**) overlaid composite SLO images produced from images on both sides; (**C**, **G**, **K**, **O**) SLO images taken immediately before preparation of retinal flatmounts; (**D**, **H**, **L**, **P**) identical retinal flatmount area to SLO images of **C**, **G**, **K**, and **O**, respectively. Newly emerged fluorescent spots were not present in control retinas, but were observed in postcrush retinas (**F**, **J**, **N**, *arrows*). Identical cells to those indicated are marked by *arrows* in **G**, **H**, **K**, **L**, **O**, and **P**. *Arrows* in retinal flatmounts indicate cells with sizes and shapes different from those of typical RGCs. Scale bar, 100 μm.

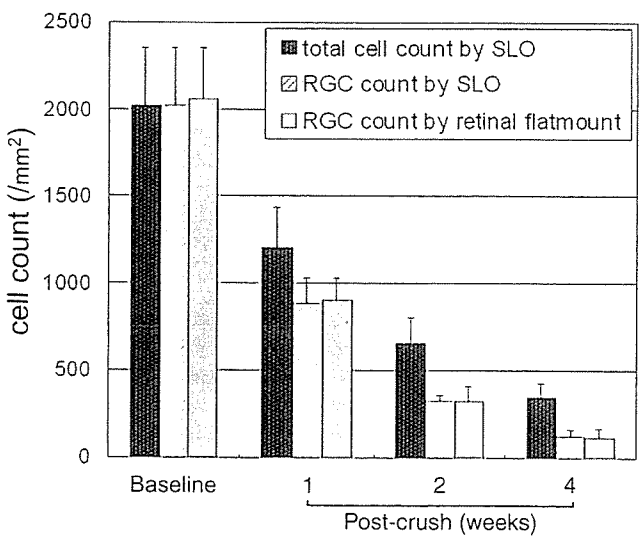

FIGURE 6. RGC counts by SLO and in retinal flatmounts. RGC counts in SLO images were determined by subtracting the number of newly emerged fluorescent cells from total cell counts. Morphologic criteria for discriminating non-RGC cells from RGCs were applied to RGC counting in retinal flatmounts. RGC counts by SLO are not significantly different from those in retinal flatmounts. Data are presented as the mean ± SD (n = 6 each).

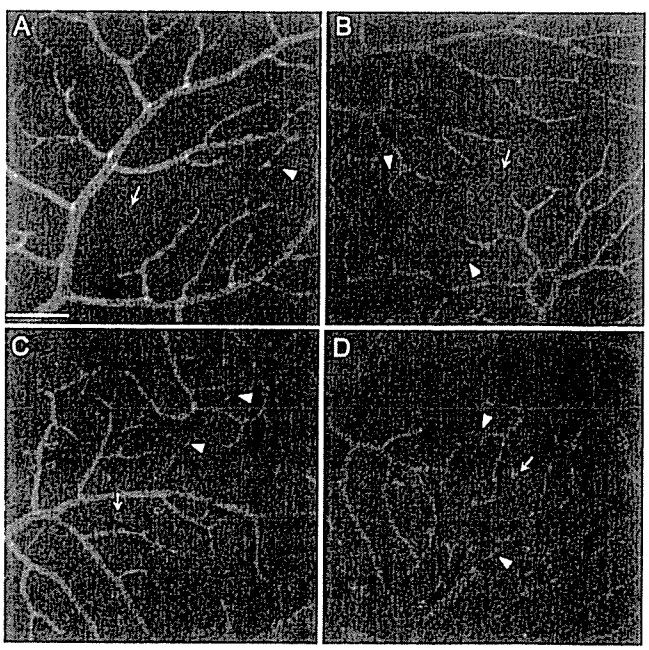

FIGURE 7. Lectin-stained microglia in retinal flatmounts. Representative photographs of retinal flatmounts at baseline (**A**), and 1 (**B**), 2 (**C**), and 4 (**D**) weeks after optic nerve crush. Lectin-stained cell bodies (*arrows*) and processes (*arrowheads*) of microglia increased after optic nerve injury, which peaked 2 weeks after the crush. Retinal vessels are also stained by lectin. Scale bar, 100 μm.

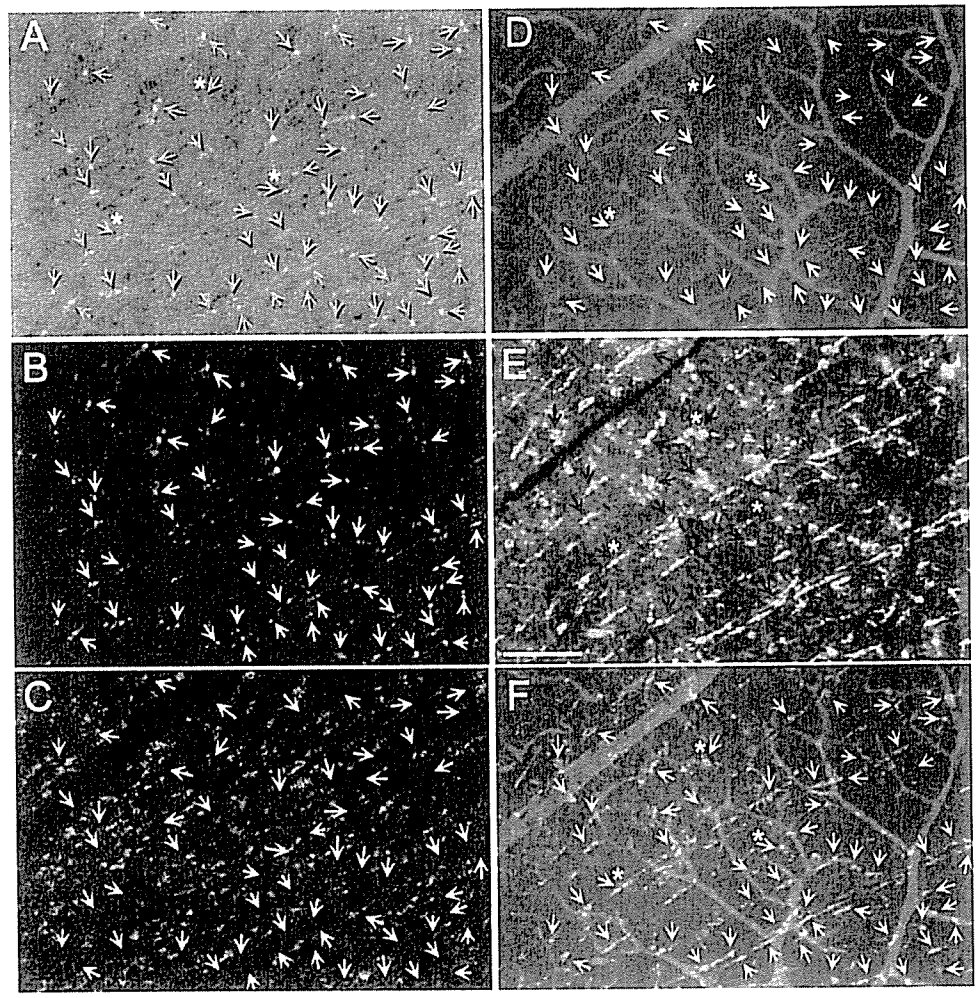

FIGURE 8. Example of point-by-point comparison of newly emerged fluorescent spots in SLO images and lectin-stained microglia. (**A**) Newly emerged fluorescent spots were marked by *arrows* in the overlaid composite images of baseline (**C**) and 2 weeks after optic nerve crush (**B**). (**B**, **C**, *arrows*) Identical positions to those in (**A**). The same retinal positions highlighted by *arrows* in (**B**) were carefully marked on the retinal flatmount showing DiA fluorescence 2 weeks after the crush (**E**). Identical *arrow* positions in (**E**) can be located on the lectin-stained flatmount (**D**) by making a superimposed image (**F**) of (**D**) and (**E**). Blood vessels showing lectin binding facilitate the correct positioning of the two images. By comparing *arrows* in (**A**) and (**D**), newly emerged fluorescent spots in SLO images appear to colocalize mostly with microglial processes and occasionally within the vicinity of microglial cell bodies (*). Scale bar, 100 μm.

ity of microglial cell bodies (Fig. 8). The colocalization was observed 1, 2, and 4 weeks after optic nerve crush.

DISCUSSION

Imaging of living RGCs in vivo has definite advantages for counting RGCs over conventional microscopic observation in flatmount retina preparations. In the histologic assessment, the number of RGCs in the selected sampling areas (usually <10% of the entire retina) are averaged and compared between eyes of the same or different rats. Accordingly, the number of RGCs and their distribution in the retina are assumed to be the same in the right and left eyes and in different animals. Also, consistent labeling of RGCs is another essential premise that can never be proven exactly until the total number of RGCs is counted. However, Danias et al.[5] pointed out the inherent problem of RGC counting by a sampling method in retinal flatmounts. They reported considerable variability of RGC density in different eyes of Wistar rats by counting RGCs in the entire retina and estimated that nearly 20 animals are necessary for the detection of a 20% difference between control and experimental eyes when 25% of the retinal area is used for cell counting. However, in vivo imaging allows repeated counting of RGCs in the same retinal area without being affected by the variability of staining and density of RGCs in different retinas. Therefore, if the same sampling procedure were used to detect the difference between pre- and posttreatment status, in vivo imaging would need fewer animals than histologic methods.

In this study, we used an SLO and repeatedly imaged RGCs successfully in vivo. Visualization of fluorescent cells in vivo with an SLO was reported by Nishiwaki et al.[12] In their study, fluorescent leukocytes stained with acridine orange were counted in rat retinas in SLO images. Similarly, fluorescent RGCs were countable in SLO images in this study.

For long-term in vivo monitoring of RGCs, carbocyanines are suitable as tracers because they are nontoxic, their labeling is intense, and labeling is stable, with survival times of up to 1 year.[17,18] Among carbocyanines, DiI (1-1′-dioctadecyl-3,3,3′,3′-tetramethylindocarbocyanine perchlorate), and 4Di-10Asp (4-(4-(didecylamino)styryl)-*N*-methylpyridinium iodine) have been used for retrograde labeling of RGCs to count RGCs in retinal flatmounts.[3,4,18] Naskar et al.[4] reported the visualization of RGCs in vivo by retrograde staining with 4Di-10Asp and fluorescence microscopy. DiA is a carbocyanine dye that is widely used as an anterograde and retrograde neuronal tracer in vivo. We chose DiA as a tracer for the SLO imaging because it has an appropriate absorption and fluorescence emission property for the argon laser and optical filter sets equipped for fluorescein angiography with an SLO. However, the labeled cell density with carbocyanines is lower than that with a hydrophilic tracer (Fluorogold; Fluorochrome, Denver, CO), probably due to lower solubility of the lipophilic dyes.[19,20] The density of DiA-labeled cells in SLO images of normal rat retinas was comparable to reported densities of RGCs stained with other carbocyanines.[4,18–20] Furthermore, the extent of decrease in of labeled cells after axonal injury agreed with that in previous

reports,[21,22] and the number of labeled cells in control eyes was constant during the experimental period. Thus, DiA is a suitable tracer for in vivo imaging of RGCs with an SLO.

We encountered several problems in SLO imaging of RGCs. First, the whole area of a single SLO frame (40°) could not be focused well simultaneously because of the image distortion by the contact lens and the spherical property of the eye. Although the minimum well-focused area was larger than the area for RGC counting in retinal flatmounts in other studies,[2,4,19,23] modification of a contact lens to enlarge the well-focused area would improve the quality of SLO images and save recording and analysis time. Second, peripheral fundus areas were difficult to image with an SLO. We selected a sampling area for RGC counting 0.5 to 1.5 mm from the center of the optic disc because of the ease of focusing. However, the adult rat retina extends more than 5 mm from the center of the optic disc.[5] Therefore, an SLO is not suitable for evaluation of RGCs in the peripheral retina.

Finally, SLO image quality was not as good as that of retinal flatmounts. Although the cell density measured in SLO images was not significantly different from that determined in flatmount images, the resolution and sensitivity of fluorescence in SLO images were lower than those in flatmount images. As reported previously, cells stained by retrograde labeling are not necessarily RGCs, because other types of cells may become labeled by phagocytosis of fluorescent RGC debris.[4,15,24] Morphologic criteria were defined to distinguish RGCs from other types of cells for counting RGCs in the retinal flatmount.[13,14,25] However, the SLO images of labeled cells were not good enough for discrimination of cell types. Thus, it may be difficult to distinguish RGCs from microglial cells morphologically and to count RGCs accurately in postcrush retina in SLO images.

To discriminate RGCs from other types of cells in SLO images, we developed a new image overlay analysis. The overlaid composite images of pre- and postcrush SLO images showed that new fluorescent spots emerged and moved after the optic nerve crush. A point-by-point comparison of the SLO image overlay and the retinal flatmount in the identical retinal area revealed that the newly emerged fluorescent spots in SLO images after the crush corresponded to non-RGC cells. Therefore, it is reasonable to determine RGC counts in SLO images by subtracting the number of newly emerged fluorescent cells from total cell counts. Furthermore, similar RGC counts by SLO and retinal flatmounts indicate that the image overlay system is useful to count RGCs in SLO images.

As newly emerged fluorescent spots are thought to be microglia that became labeled by phagocytosis of dead RGCs, we compared the SLO image overlay and lectin staining of microglia in retinal flatmounts. Colocalization of most of the new fluorescent spots with microglial processes indicated that image overlay analysis can be useful to monitor the activity of microglia after optic nerve injury.

In conclusion, the SLO is useful for in vivo imaging and counting of rat RGCs and may be a valuable tool for monitoring RGC changes over time in various rat models of RGC damage. This approach will be useful for studying the pathology of optic neuropathy including glaucoma and for developing new therapies.

References

1. Goldblum D, Mittag T. Prospects for relevant glaucoma models with retinal ganglion cell damage in the rodent eye. *Vision Res.* 2002;42:471-478.
2. Villegas-Perez MP, Vidal-Sanz M, Bray GM, Aguayo AJ. Influences of peripheral nerve grafts on the survival and regrowth of axotomized retinal ganglion cells in adult rats. *J Neurosci.* 1988;8:265-280.
3. Yoles E, Schwartz M. Degeneration of spared axons following partial white matter lesion: implications for optic nerve neuropathies. *Exp Neurol.* 1998;153:1-7.
4. Naskar R, Wissing M, Thanos S. Detection of early neuron degeneration and accompanying microglial responses in the retina of a rat model of glaucoma. *Invest Ophthalmol Vis Sci.* 2002;43:2962-2968.
5. Danias J, Shen F, Goldblum D, et al. Cytoarchitecture of the retinal ganglion cells in the rat. *Invest Ophthalmol Vis Sci.* 2002;43:587-594.
6. Sabel BA, Engelmann R, Humphrey MF. In vivo confocal neuroimaging (ICON) of CNS neurons. *Nat Med.* 1997;3:244-247.
7. Thanos S, Indorf L, Naskar R. *In vivo* FM: using conventional fluorescence microscopy to monitor retinal neuronal death *in vivo*. *Trends Neurosci.* 2002;25:441-444.
8. Paques M, Genevois O, Regnier A, et al. Axon-tracing properties of indocyanine green. *Arch Ophthalmol.* 2003;121:367-370.
9. Cordeiro MF, Guo L, Luong V, et al. Real-time imaging of single nerve cell apoptosis in retinal neurodegeneration. *Proc Natl Acad Sci USA.* 2004;101:13352-13356.
10. Miglior S, Rossetti L, Brigatti L, Bujtar E, Orzalesi N. Reproducibility of retinal nerve fiber layer evaluation by dynamic scanning laser ophthalmoscopy. *Am J Ophthalmol.* 1994;118:16-23.
11. Sugiyama K, Uchida H, Tomita G, et al. Localized wedge-shaped defects of retinal nerve fiber layer and disc hemorrhage in glaucoma. *Ophthalmology.* 1999;106:1762-1767.
12. Nishiwaki H, Ogura Y, Kimura H, Kiryu J, Honda Y. Quantitative evaluation of leukocyte dynamics in retinal microcirculation. *Invest Ophthalmol Vis Sci.* 1995;36:123-130.
13. Chauhan BC, LeVatte TL, Jollimore CA, et al. Model of endothelin-1-induced chronic optic neuropathy in rat. *Invest Ophthalmol Vis Sci.* 2004;45:144-152.
14. Levkovitch-Verbin H, Quigley HA, Martin KRG, Zack DJ, Pease ME, Valenta DF. A model to study differences between primary and secondary degeneration of retinal ganglion cells in rats by partial optic nerve transaction. *Invest Ophthalmol Vis Sci.* 2003;44:3388-3393.
15. Streit WJ. An improved staining method for rat microglial cells using the lectin from Griffonia simplicifolia (GSA I-B4). *J Histochem Cytochem.* 1990;38:1683-1686.
16. Garcia-Valenzuela E, Sharma SC, Pina AL. Multilayered retinal microglial response to optic nerve transsection in rats. *Mol Vis.* 2005;11:225-231.
17. Kobbert C, Apps R, Bechmann I, Lanciego JL, Mey J, Thanos S. Current concept in neuroanatomical tracing. *Prog Neurobiol.* 2000;62:327-351.
18. Vidal-Sanz M, Villegas-Perez MP, Bray GM, Aguayo AJ. Persistent retrograde labeling of adult rat retinal ganglion cells with the carbocyanine dye dil. *Exp Neurol.* 1988;102:92-101.
19. Lafuente MP, Villegas-Perez MP, Selles-Navarro I, Mayor-Torroglosa S, Miralles de Imperial J, Vidal-Sanz M. Retinal ganglion cell death after acute retinal ischemia is an ongoing process whose severity and duration depends on the duration of the insult. *Neuroscience.* 2002;109:157-168.
20. Simon P, Thanos S. Combined methods of retrograde staining, layer-separation and viscoelastic cell stabilization to isolate retinal ganglion cells in adult rats. *J Neurosci Methods.* 1998;83:113-124.
21. Villegas-Perez MP, Vidal-Sanz M, Rasminsky M, Bray GM, Aguayo AJ. Rapid and protracted phases of retinal ganglion cell loss follow axotomy in the optic nerve of adult rats. *J Neurobiol.* 1993;24:23-36.
22. Selles-Navarro I, Ellesam B, Fajardo R. Retinal ganglion cell and nonneural cell responses to a microcrush lesion of adult rat optic nerve. *Exp Neurol.* 2001;167:282-289.
23. Klocker N, Cellerino A, Bahr M. Free radical scavenging and inhibition of nitric oxide synthase potentiates the neurotrophic effects of brain-derived neurotrophic factor on axotomized retinal ganglion cells *in vivo*. *J Neurosci.* 1998;18:1038-1046.
24. Thanos S, Kacza J, Seeger J, Mey J. Old dyes for new scopes: the phagocytosis-dependent long-term fluorescence labeling of microglial cells *in vivo*. *Trends Neurosci.* 1994;17:177-182.
25. Perry VH, Henderson Z, Linden R. Postnatal changes in retinal ganglion cell and optic axon populations in the pigmented rat. *J Comp Neurol.* 1983;219:356-368.

Available online at www.sciencedirect.com
ScienceDirect
Experimental Eye Research 83 (2006) 1317–1324
EXPERIMENTAL EYE RESEARCH
www.elsevier.com/locate/yexer

Pharmacological vascular reactivity in isolated diabetic rabbit ciliary artery

Toshiaki Goseki [a,*], Hitoshi Ishikawa [b], Hisaharu Nishimoto [a], Kimiyo Mashimo [a], Shigekazu Uga [c], Takeshi Yoshitomi [d], Kimiya Shimizu [a]

[a] *Department of Ophthalmology, Kitasato University School of Medicine, 1-15-1 Kitasato, Sagamihara, Kanagawa 228-8555, Japan*
[b] *Department of Orthoptics and Visual Science, School of Allied Health sciences, Kitasato University, Kanagawa, Japan*
[c] *Department of Ophthalmology, International University of Health and Welfare, Tochigi, Japan*
[d] *Department of Ophthalmology, Akita University School of Medicine, Akita, Japan*

Received 2 November 2005; accepted in revised form 4 June 2006
Available online 18 September 2006

Abstract

Impairment of the ocular circulation induced by diabetes mellitus has not been fully defined, but is thought to be related to hemodynamic changes in the ocular circulation. The purpose of the present study is to investigate the functional and morphological changes occurring in the ciliary artery wall of rabbits with alloxan-induced diabetes mellitus. A single intravenous bolus injection of alloxan (100 mg/kg) was given to each of 26 10-week-old rabbits and 16 sham-injected control rabbits. Twenty weeks later, control rabbits and diabetic rabbits were sacrificed, and their ciliary arteries were mounted in a myograph system. The responses of these arteries to high K^+ solution (K-Krebs solution), phenylephrine and carbachol were investigated using isometric tension recording. L-NAME (*NG*-nitro-L-arginine methyl ester; 100 μM) and indomethacin (1 μM) were also used to test the mechanism causing the carbachol induced relaxation. The arteries were also examined morphologically. The maximum tensions induced by K-Krebs solution in this tissue were not significantly different: 17.2 ± 0.8 mN ($n = 16$) in the control rabbits and 17.6 ± 0.8 mN ($n = 23$) in the diabetic rabbits ($P = 0.36$). Phenylephrine caused dose-dependent contraction with EC_{50} values of 1.3 ± 0.4 μM ($n = 6$) in the control and 5.1 ± 2.3 μM ($n = 6$) in the diabetic rabbits, but there was no significant difference between the two ($P = 0.36$). Carbachol induced dose-dependent relaxations in segments precontracted with K-Krebs solution. These relaxations were significantly reduced in the diabetic rabbits. The maximum relaxation induced by carbachol was 77.0 ± 2.4% (10 μM) and 66.4 ± 2.5% (100 μM) in the control and diabetic rabbits, respectively. These values were significantly different ($P = 0.0076$). The IC_{50} value for carbachol was 396.3 ± 58.4 nM ($n = 16$) in the control, and 443.6 ± 141.1 nM ($n = 23$) in the diabetic rabbit ($P = 0.87$). Application of a 100 μM nitric oxide synthase inhibitor, L-NAME, significantly inhibited the amplitude of relaxations evoked by carbachol ($P = 0.0066$). However, these relaxations were not inhibited by pretreatment with 1 μM indomethacin ($P = 0.60$). Histologically, the frequency of invaginations was less in the diabetic arterioles with a flattening of the lamina in the diabetic rabbits than in the controls. The cytoplasm of endothelial cells contained large vacuoles, indicating weak adhesion to the lamina. Some endothelial cells even showed vacuolar degeneration due to breakdown of the cell membranes. However, the smooth muscle cells were well preserved in the diabetic rabbit. These results suggest that the mechanism of impairment of ocular circulation induced by diabetes mellitus is mainly the reduction of NO synthase due to endothelial cell dysfunction. Furthermore, the characteristics of rabbits with alloxan-induced diabetes mellitus probably make them a useful model for investigating ocular complications induced by diabetic mellitus.

Keywords: rabbit; ciliary artery; alloxan; diabetes mellitus; ocular circulation; vasodilatation; vasoconstriction

* Corresponding author. Tel.: +81 42 778 8464; fax: +81 42 778 2357.
E-mail address: gosekikun@aol.com (T. Goseki).

0014-4835/$ - see front matter © 2006 Elsevier Ltd. All rights reserved.
doi:10.1016/j.exer.2006.06.001

1. Introduction

There are many factors that influence the ocular circulation, for example, diabetes mellitus, hypercholesterolemia and hypertension. One of the major concerns in the long-term management of diabetes is the development of chronic complications. Diabetes mellitus is a very commonly seen risk factor in the development of non-arteritic anterior ischemic optic neuropathy (Kelman, 1998). Impairment of vascular reactivity has been demonstrated in diabetic animals and humans, and has been studied using streptozotocin-induced hyperglycemic rats and alloxan-induced hyperglycemic rabbits as diabetic models. (Taylor et al., 1992; Tesfamariam et al., 1989; Yu et al., 1998, 2001; Masuda et al., 1999).

Since the original observations of Furchgott and Zawadzki (1980), it has been demonstrated that the vascular endothelium plays an important role in the regulation of vascular tonus. Various agents are reported to generate relaxation through the activation of endothelium-derived relaxing factor (EDRF), which is now recognized to be nitric oxide (NO) (Ignarro et al., 1987; Palmer et al., 1987). The majority of studies have focused on the role of NO. However, it is becoming clear that other factors, such as endothelium-derived hyperpolarizing factor (EDHF), may play a role. The importance of this lies in the fact that, whereas in large vessels NO is the predominant endothelial vasodilator, in many smaller arteries EDHF assumes a prominent role in endothelium-dependent vasodilatation (Shimokawa et al., 1996; Busse et al., 2002; Fitzgerald et al., 2005).

Many investigators have reported functional alterations of the vascular endothelial cells that are related to hypertension (Luscher and Vanhoutte, 1986), hyperlipidemia (Ishikawa et al., 2004; Verbeuren et al., 1986), atherosclerosis (Jayakody et al., 1987), and diabetes (Kamata et al., 1989; Abiru et al., 1990). Previous work on endothelium-dependent relaxation in diabetic animals has demonstrated controversial responses in different vascular beds (Wakabayashi et al., 1987; Kamata et al., 1989; Abiru et al., 1990; Forti and Fonteles, 1998). Yu et al. (2001) reported that the acetylcholine-induced vasodilatation response is impaired in the ocular microvasculature of rats with streptozotocin-induced diabetes. Moreover, exogenous tetrahydrobiopterin reversed the endothelium impairment in this model.

The present study was initiated to investigate the functional and morphological changes occurring in the vascular wall with alloxan-induced diabetes in the isolated rabbit ciliary artery. The data obtained from the diabetic rabbits was compared with age-matched control rabbit data.

2. Materials and methods

2.1. General

Experiments were conducted in accordance with the ARVO Resolution on the Use of Animals in Research. Forty-two male Japanese White rabbits were used. They were purchased at 8 weeks of age and were housed in a temperature- and humidity-controlled room (24–25 °C, 55–60%). They were fed regular chow (120 g/day of CR-1, Clea, Tokyo, Japan) throughout the experimental period. A single intravenous bolus injection of alloxan (100 mg/kg) in 0.9% w/v saline was given via the marginal ear vein to 26 rabbits aged 10 weeks. Age-matched control rabbits ($n = 16$) were injected with a similar volume of saline. We measured blood glucose and weight once a week.

Twenty weeks after the alloxan injection, age-matched control rabbits and diabetic rabbits were sacrificed by administration of an overdose of intravenous pentobarbital sodium (Abbot, North Chicago, IL, USA).

2.2. Ring segment preparation and mounting

The eyes were immediately enucleated with care to remove a maximum length of optic nerve. The specimens were placed in oxygenated Krebs solution that contained the following (mM): NaCl 94.8, KCl 4.7, $MgSO_4$ 1.2, $CaCl_2$ 2.5, KH_2PO_4 1.2, $NaHCO_3$ 25.0, and glucose 11.7. The ciliary artery with its connective tissue was carefully dissected free from the optic nerve. Vascular segments (200–300 μm in diameter, 1–2 mm in length) were cut from the distal section of the ciliary artery and mounted in a double myograph system (JP Trading, Denmark) under microscopic observation (Nyborg et al., 1990). An arterial specimen was prepared from one animal only.

This myograph system allows direct determination of the isometric tension of the vessels while the internal circumference is controlled. The vessels were equilibrated for 30 min in oxygenated Krebs solution with 5% CO_2 and 95% O_2 at 37 °C. Detailed methods for isometric tension recording with a myograph system have been described by Mulvany and Halpern (1977).

2.3. Functional examinations

After the mounting and equilibration of the artery specimen, K-Krebs solution prepared by isotonically replacing equimolar NaCl with KCl ($K^+ = 100.7$ mM) was introduced three times into the chamber, causing three sequential contractions in the specimen with replacement of normal Na-Krebs solution in between each contraction. The isometric tensions of each of these contractions were measured at 90-min intervals to establish the viability and stability of the preparation. During the contractions, it was confirmed that 10 μM carbachol induced relaxation in all preparations, which indicated that the endothelium in each preparation was intact.

Phenylephrine (PE) was added cumulatively into the organ-bath. Indomethacin (1 μM) and *NG*-nitro-L-arginine methyl ester (L-NAME) (100 μM) were added to the bath 20 min before the start of administration of carbachol.

2.4. Morphological examinations

Segments of the ciliary specimens not used for the functional studies were fixed by immersion in 10% phosphate-buffered

formalin and were then embedded in paraffin. From each specimen, serial sections were cut and then stained with hematoxylin and eosin. For transmission electron microscopy, the extracted arterial specimens were fixed overnight with 4% glutaraldehyde buffered with 0.075 M phosphate solution. After being washed in buffer, these specimens were post-fixed overnight with 1% OsO_4 in the same buffer solution, dehydrated in an ethanol series, and embedded in Quetol 812. After polymerization, the specimens were cut with a Reichert-Nissei Ultratome (Ultracut N, Reichert Optische Werke AG, Vienna, Austria). These sections were stained with lead citrate and uranyl acetate and examined with an electron microscope (HU-12A, Hitachi, Tokyo). Some of the specimens were intended for scanning electron microscopy and so were transferred to isoamyl acetate. After critical-point drying, they were sputtered with gold, and examined in a scanning electron microscope.

2.5. Data analysis

The EC_{50} and IC_{50} values were calculated using nonlinear regression fits performed with Prism (GraphPad, San Diego, CA. USA) and were presented as means ± S.E. Statistical differences between points were determined by the Mann–Whitney *U*-test, and between the concentration–response curves by repeated-measures ANOVA with a post hoc test. $P < 0.05$ was considered significant.

2.6. Chemicals

The following drugs were used: carbachol hydrochloride and alloxan HCl (Sigma–Aldrich Co., St Louis, MO, USA), phenylephrine (PE; Wako Chemical Inc., Osaka, Japan), *NG*-nitro--arginine methyl ester (L-NAME; Wako Chemical, Osaka, Japan), indomethacin (Banyu Pharmaceutical Co. Ltd., Tokyo, Japan). All chemicals were of reagent grade.

3. Results

3.1. Baseline data

We administered alloxan to 26 rabbits. Two out of the 26 died of a hypoglycemic attack the following day. One of the alloxan treated rabbits did not develop hyperglycemia. Table 1 shows the body weight change rate and plasma blood glucose levels in experimental rabbits. Diabetic rabbits, especially those with glucose levels more than 600 mg/dl, did not increased their body weights compared with age-matched control rabbits (Table 1).

3.2. Contractile activity

When specimens of the ciliary artery were mounted in the organ bath, the tissue gradually relaxed to a steady tone after 0.5–1 h superfusion with Krebs solution. No spontaneous contractions occurred during the experiment. The maximum tensions developed by K-Krebs solution in this tissue were 17.2 ± 0.8 mN ($n = 16$) in the control rabbits and 17.6 ± 0.8 mN ($n = 23$) in the diabetic rabbits, showing no significant difference between the two ($P = 0.36$). PE that was exogenously applied to six rabbits caused dose-dependent contraction in this tissue (Fig. 1). The EC_{50} values were 1.3 ± 0.4 μM ($n = 6$) in the control rabbits and 5.1 ± 2.3 μM ($n = 6$) in the diabetic rabbits, showing no significant difference ($P = 0.37$).

Table 1
Plasma blood glucose levels and weight change rate

Plasma glucose	Weight change (%)
Control: 85–134 mg/dl ($n = 16$)	146.1 ± 4.2
<200 mg/dl[a] ($n = 1$)	159.5
200–600 mg/dl ($n = 12$)	135.3 ± 3.2
>600 mg/dl ($n = 11$)	104.5 ± 3.4
Total ($n = 24$[b])	

Blood glucose values were at the maximum level during follow-up. They were non-fasting values. Weight change rate (%) = weight at time of sacrifice (kg)/weight before alloxan administration (kg) × 100.

[a] Data on plasma blood glucose levels less than 200 mg/dl were excluded from this study.

[b] We have injected alloxan in 26 rabbits. Two rabbits died of hypoglycemia.

3.2.1. Mechanical responses to carbachol

After pre-contraction by K-Krebs solution, carbachol provoked relaxation in a dose-dependent manner in both control and diabetic rabbits (Fig. 2). Fig. 2 shows the dose–response relationship of carbachol in the rabbit ciliary artery pre-contracted with K-Krebs solution, where the amplitude of contraction that was evoked by such solutions was defined as the relative amplitude of 100%. The relaxation response was significantly reduced in diabetic segments. The maximum relaxation induced by carbachol was 77.0 ± 2.4% (10 μM) and 66.4 ± 2.5% (100 μM) in the control and diabetic rabbits, respectively. These values were significantly different ($P = 0.0076$). The IC_{50} value was 396.3 ± 58.4 nM ($n = 16$) in the control, and 443.6 ± 141.1 nM ($n = 23$) in the diabetic rabbit ($P = 0.87$).

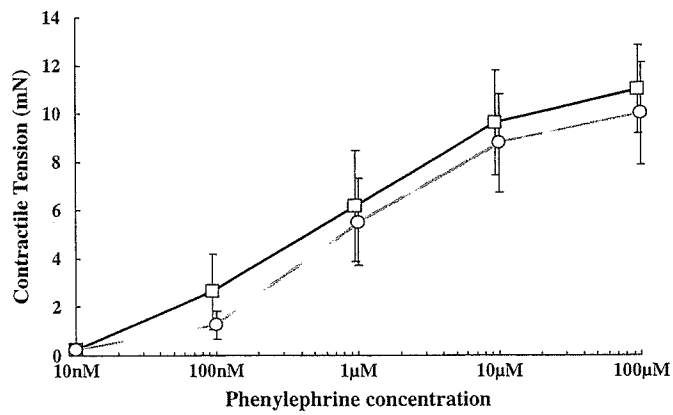

Fig. 1. Dose–response curves in the diabetic rabbit (open squares, $n = 6$), age-matched control (open circles, $n = 6$) ciliary arteries for phenylephrine. The bars show S.E.M. The maximum contraction induced by phenylephrine was 10.0 ± 2.1 mN and 11.3 ± 1.8 mN in the control and diabetic rabbits, respectively. There was no significant difference between the two ($P = 0.30$).

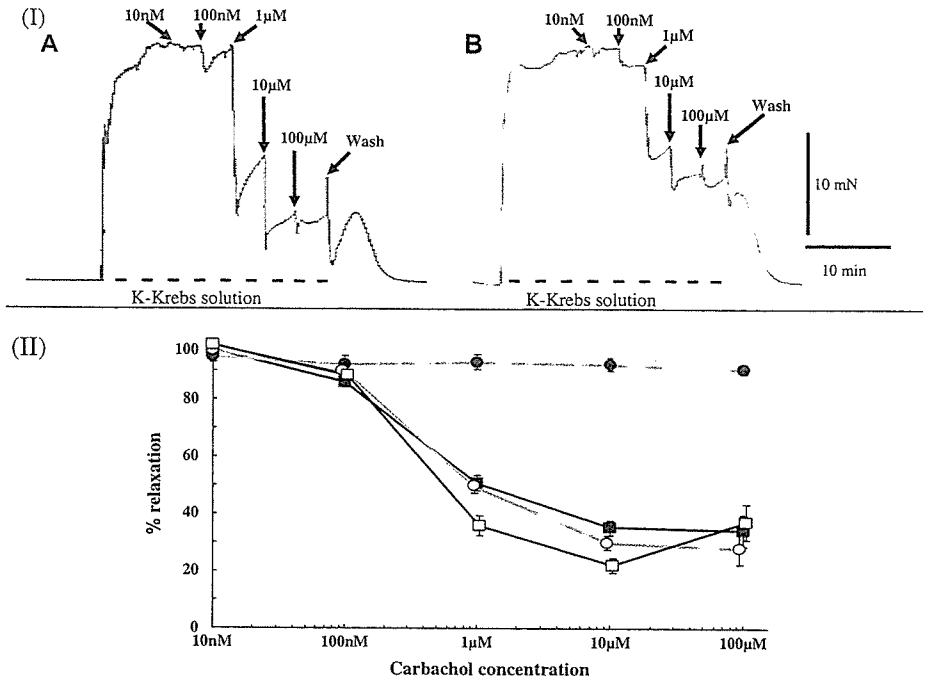

Fig. 2. (I) Typical tracing showing effects of cumulative application of carbachol to the rabbit ciliary artery (diameter 200–300 μM) pre-contracted with K-Krebs solution. (A) Control; (B) diabetes. (II) Dose–response relationships of carbachol applied to diabetes (closed squares, carbachol alone ($n = 23$); open circles, carbachol with 1 μM of indomethacin ($n = 6$); closed circles, carbachol with 100 μM of L-NAME ($n = 6$)) and age-matched control (open squares, $n = 16$) rabbit ciliary artery pre-contracted with K-Krebs. The bars show S.E.M.

Carbachol induced relaxation only in preparations with an intact endothelium, and had no effect on preparations lacking the endothelium (data not shown). Application of a nitric oxide synthase inhibitor (L-NAME, 100 μM) inhibited the amplitude of relaxation evoked by carbachol ($P = 0.0066$, Fig. 2). However, relaxation evoked by carbachol was not inhibited by pretreatment with 1 μM indomethacin ($P = 0.60$, Fig. 2).

3.3. Morphologic changes

Histologically, the cross-section of the rabbit ciliary artery in the age-matched control showed relatively regular invaginations of internal elastic lamina, whereas in the diabetic rabbit ciliary artery, invaginations of the internal elastic lamina clearly decreased. However, the size of the lumen was almost the same in both arteries (Fig. 3).

Electron-microscopically, deep invaginations of the internal elastic lamina in the control group were confirmed. The frequency of invaginations in the arteries of diabetic rabbits was relatively low, and the lamina was flattened. Furthermore, the cytoplasms of endothelial cells contain large vacuoles, indicating weak adhesion to the lamina. However, the smooth muscle cells were well preserved (Fig. 4). Some endothelial cells even showed vacuolar degeneration due to breakdown of their cell membranes (Fig. 5). Scanning electron-microscopic observations showed that the internal surface of the artery in the control group consisted of endothelial cells of a constant width, while that of the diabetic rabbits comprised irregularly arranged cells of varying sizes (Fig. 6). In the diabetic group, a network, considered to consist of fibrin, was

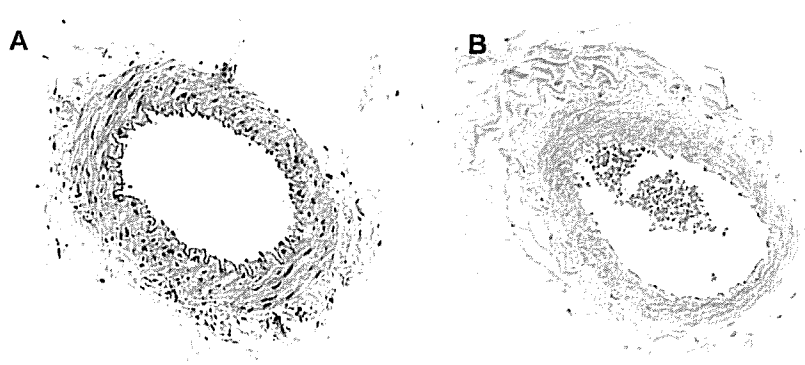

Fig. 3. Morphological cross-section (×200) of representative age-matched control (A) and diabetic (B) rabbit ciliary arteries.

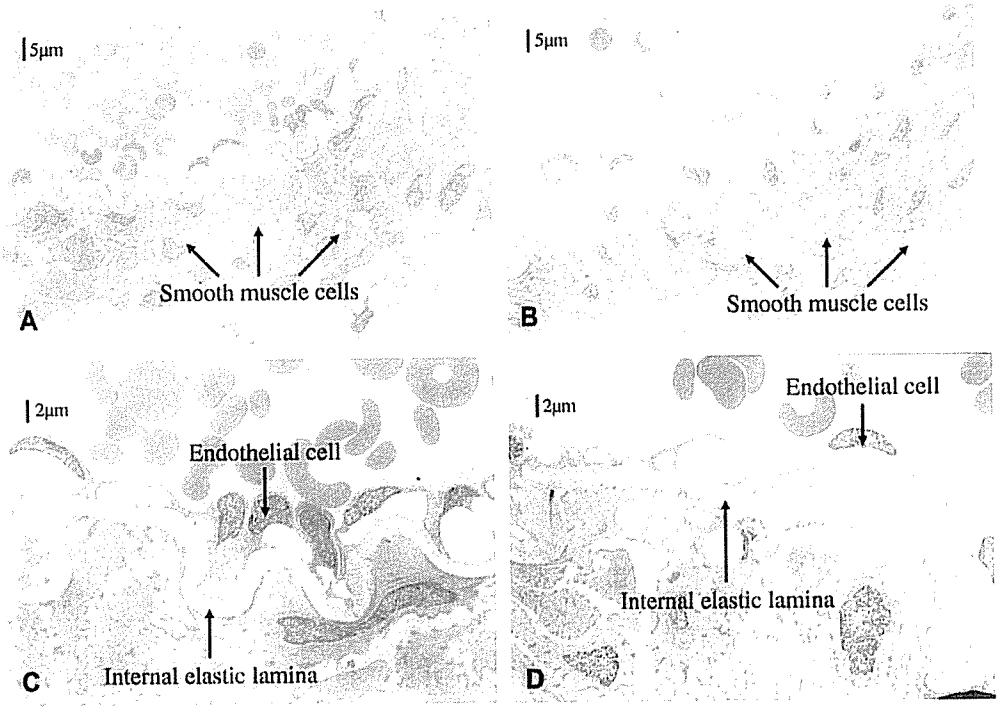

Fig. 4. Transmission electron micrographs comparing age-matched control (A, C) and diabetic (B, D) rabbit ciliary arteries. (A, B: ×1000; C, D: ×2500).

seen on the internal surface of the arteries, adhering to the endothelial cells (Fig. 6).

4. Discussion

4.1. Alloxan-induced DM

Dysfunction of vascular control is a common complication of diabetes mellitus. In the present study, an intravenous bolus injection of alloxan (100 mg/kg) induced hyperglycemia in 24 rabbits out of 26. Two rabbits died of hypoglycemia. The remaining rabbit showed normoglycemia, indicating variability in the susceptibility of rabbits to alloxan. Alloxan injections are known to induce pancreatic damage, the changes consisting mainly of selective necrosis and disappearance of the beta cells with consequent destruction of the architecture of the islets (Lazarow and Palay, 1946; Lukens, 1948). Diabetes mellitus was induced by this mechanism. Body weight loss was reported in many cases in alloxan-induced animal models, and our data of body weight changes supported these previous studies (Abiru et al., 1990; Tesfamariam and Cohen, 1995; Masuda et al., 1999). Humans are similar in that most type 1 diabetic patients are ill and symptomatic, most commonly presenting with polyuria, polydipsia, polyphagia, and weight loss (Sherwin, 2004).

4.2. Functional findings

In the present study, there was no significant difference in the average maximum tension developed by K-Krebs solution, between the control and diabetic rabbits. Moreover, PE caused dose-dependent contraction, the EC_{50} values and maximum contraction induced by PE were not significantly different between control and diabetic rabbit. The lack of any effect of diabetes on PE-induced contraction suggests that physiological antagonism of this response by endothelium-derived NO is not observed in rabbit ciliary arteries in a static system, but only in a perfused system. Similar observations have been made in bovine ciliary arteries (Buckley et al., 1998).

Sullivan and Sparks (1979) found decreased vascular response to norepinephrine in isolated diabetic rabbit aortas, while Christlieb (1974) found normal vascular sensitivity in diabetic rats. Moreover, the responses to endogenous noradrenalin released from adrenergic nerves by electrical stimulation did not differ between arteries from normal and diabetic

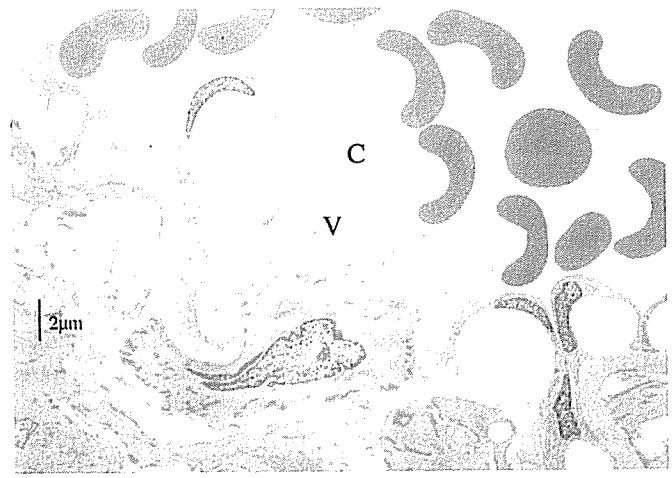

Fig. 5. Transmission electron micrographs (×3000). Loss of endothelial cells (C) in contact with vacuolar degeneration (V) in diabetic rabbit ciliary artery.